DEVELOPMENTAL BIOLOGY

Deficient histone H3 propionylation by BRPF1-KAT6 complexes in neurodevelopmental disorders and cancer

Kezhi Yan[1,2], Justine Rousseau[3], Keren Machol[4,5], Laura A. Cross[6], Katherine E. Agre[7], Cynthia Forster Gibson[8], Anne Goverde[9], Kendra L. Engleman[6], Hannah Verdin[10], Elfride De Baere[10], Lorraine Potocki[4,5], Dihong Zhou[6], Maxime Cadieux-Dion[6], Gary A. Bellus[11], Monisa D. Wagner[12], Rebecca J. Hale[7], Natacha Esber[13], Alan F. Riley[14], Benjamin D. Solomon[15], Megan T. Cho[15], Kirsty McWalter[15], Roy Eyal[16], Meagan K. Hainlen[6], Bryce A. Mendelsohn[16], Hillary M. Porter[17], Brendan C. Lanpher[7], Andrea M. Lewis[4,5], Juliann Savatt[12], Isabelle Thiffault[6,18], Bert Callewaert[10], Philippe M. Campeau[3]*, Xiang-Jiao Yang[1,2,19,20]*

Copyright © 2020 The Authors, some rights reserved; exclusive licensee American Association for the Advancement of Science. No claim to original U.S. Government Works. Distributed under a Creative Commons Attribution NonCommercial License 4.0 (CC BY-NC).

Lysine acetyltransferase 6A (KAT6A) and its paralog KAT6B form stoichiometric complexes with bromodomain- and PHD finger-containing protein 1 (BRPF1) for acetylation of histone H3 at lysine 23 (H3K23). We report that these complexes also catalyze H3K23 propionylation in vitro and in vivo. Immunofluorescence microscopy and ATAC-See revealed the association of this modification with active chromatin. *Brpf1* deletion obliterates the acylation in mouse embryos and fibroblasts. Moreover, we identify *BRPF1* variants in 12 previously unidentified cases of syndromic intellectual disability and demonstrate that these cases and known *BRPF1* variants impair H3K23 propionylation. Cardiac anomalies are present in a subset of the cases. H3K23 acylation is also impaired by cancer-derived somatic *BRPF1* mutations. Valproate, vorinostat, propionate and butyrate promote H3K23 acylation. These results reveal the dual functionality of BRPF1-KAT6 complexes, shed light on mechanisms underlying related developmental disorders and various cancers, and suggest mutation-based therapy for medical conditions with deficient histone acylation.

INTRODUCTION

Histone modifications such as acetylation, phosphorylation, and methylation are critical for epigenetic regulation (*1*). Mass spectrometry has recently identified acetylation-like acylation, including propionylation, crotonylation, butyrylation, and succinylation (*2*, *3*). These modifications exhibit functional difference from acetylation in vitro and may serve as fine-tuning mechanisms in vivo. For example, both acetylation and crotonylation are recognized by the bromodomains, plant homeodomain-linked (PHD) fingers, and YEATS domains, albeit at different specificity and affinity (*3*–*7*). Like acetylation, the new acylations are reversible, but their responsible enzymes are largely unknown. Although some in vitro studies show that acetyltransferases and deacetylases also catalyze and reverse the acylations, respectively (*2*, *3*), the biological relevance remains unclear. Moreover, it is important to elucidate if and how the new acylations are linked to disease.

Lysine acetyltransferase 6A (KAT6A) and KAT6B are paralogous acetyltransferases of the MYST (Moz-, Ybf2/Sas3-, Sas2-, and Tip60-like domain) family, with similar molecular activities in vitro but distinct functions in vivo (*8*). The other three members are KAT5, KAT7, and KAT8 (*8*). Although they have conserved MYST domains for acetyltransferase activity (*8*, *9*), these five enzymes show site specificity in vivo. KAT6A and KAT6B govern acetylation of histone H3 at lysine 23 (H3K23) (*10*–*12*), whereas KAT7 is the major enzyme for H3K14 acetylation (*13*–*15*) and KAT8 is responsible for H4K16 acetylation (*16*–*19*). This specificity is conferred by multisubunit complexes. For example, KAT6A and KAT6B form tetrameric complexes with BRPF1 (bromodomain- and PHD finger–containing protein 1) and two other proteins (Fig. 1A) (*20*, *21*). BRPF1, in turn, activates KAT6A and KAT6B for H3K23 acetylation (*20*–*22*).

As for pathological relevance, *KAT6A* was identified in 1996 as a gene rearranged in leukemia (*8*, *23*). *KAT6B* was then shown to be similarly rearranged in leukemia (*8*, *23*). In 2012 and 2015, they were reported to be mutated in individuals with intellectual disability and neurodevelopmental disorders (*24*–*30*). A recent study analyzed 76 individuals with *KAT6A* variants (*31*), and at least 210 persons with these variants have enrolled in the KAT6A Foundation. Known cases with *KAT6B* variants have also exceeded 60 (*32*). We and others have just identified *BRPF1* variants in 28 individuals with syndromic intellectual disability (*12*, *33*–*36*). The variants cause deficient H3K23 acetylation (*12*, *33*). This site is also propionylated (*3*), but the enzymes are elusive. Here, we identify BRPF1-KAT6 complexes as the propionyltransferases in vitro and in vivo, demonstrate H3K23 propionylation deficiency resulting from germline *BRPF1* variants in individuals with neurodevelopmental disorders or from somatic mutations in different types of cancer,

[1]Rosalind and Morris Goodman Cancer Research Center, McGill University, Montreal, Quebec H3A 1A3, Canada. [2]Department of Medicine, McGill University, Montreal, Quebec H3A 1A3, Canada. [3]Department of Pediatrics, Sainte-Justine Hospital, University of Montreal, Quebec H3T 1C5, Canada. [4]Department of Molecular and Human Genetics, Baylor College of Medicine, One Baylor Plaza, Houston, TX 77030, USA. [5]Texas Children's Hospital, 6701 Fannin Street, Houston, TX 77030, USA. [6]Center for Pediatric Genomic Medicine and Department of Clinical Genetics, Children's Mercy Hospital, Kansas City, MO 64108, USA. [7]Department of Clinical Genomics, Mayo Clinic, Rochester, MN 55905, USA. [8]Trillium Health Partners, Credit Valley Hospital, Genetics Program, 2200 Eglinton Ave. W, Mississauga, Ontario L5M 2N1, Canada. [9]Department of Clinical Genetics, Erasmus MC, University Medical Center, Rotterdam, Netherlands. [10]Center for Medical Genetics, Ghent University and Ghent University Hospital, C. Heymanslaan 10, B-9000 Ghent, Belgium. [11]Clinical Genetics and Genomic Medicine, Geisinger, 100 N. Academy Ave., Danville, PA 17822, USA. [12]Autism and Developmental Medicine Institute, Geisinger, 120 Hamm Dr., Lewisburg, PA 17837, USA. [13]KAT6A Foundation, 3 Louise Dr., West Nyack, NY 10994, USA. [14]Texas Children's Hospital, 6651 Main Street Legacy Tower, 21st Floor Houston, TX 77030, USA. [15]GeneDx, 207 Perry Parkway, Gaithersburg, MD 20877, USA. [16]Kaiser Oakland Medical Center 3600 Broadway, Oakland, CA 94611, USA. [17]Department of Genetics and Metabolism, Rare Disease Institute, Children's National Hospital, 111 Michigan Avenue NW, Washington, DC 20010, USA. [18]Faculty of Medicine, University of Missouri Kansas City, Kansas City, MO 64110, USA. [19]Department of Biochemistry, McGill University, Montreal, Quebec H3A 1A3, Canada. [20]McGill University Health Center, Montreal, Quebec H3A 1A3, Canada. *Corresponding author. Email: p.campeau@umontreal.ca (P.M.C.); xiang-jiao.yang@mcgill.ca (X.-J.Y.)

Downloaded from http://advances.sciencemag.org/ on February 12, 2020

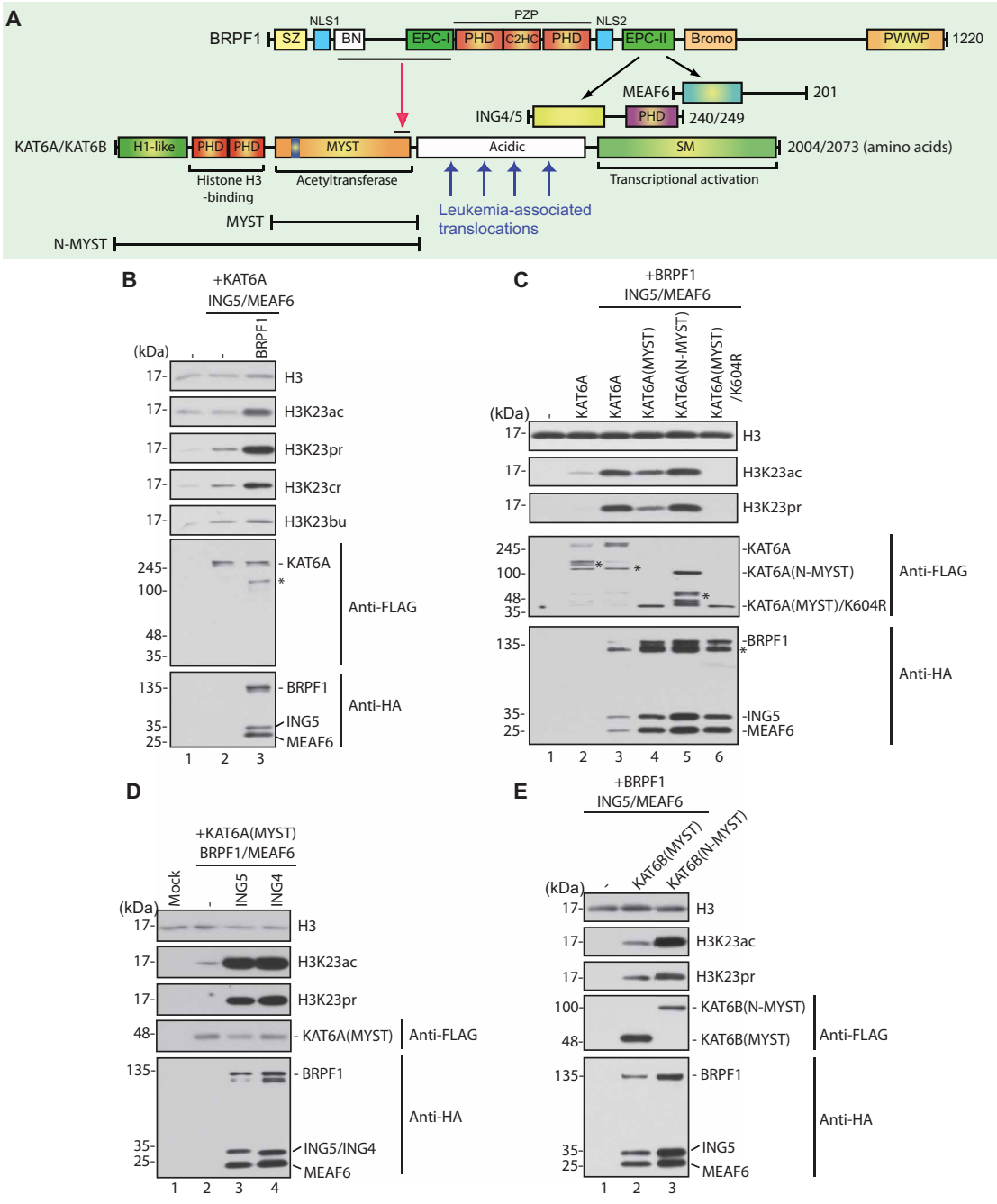

Fig. 1. BRPF1-KAT6 complexes catalyze H3K23 propionylation in vitro. (**A**) Molecular architecture of the tetrameric complexes. BRPF1 has two EPC (enhancer of polycomb)–like motifs: EPC-I is required for association with the MYST domain of KAT6A or KAT6B, whereas EPC-II is necessary and sufficient for interaction with ING5 (or the paralog ING4) and MEAF6. The BRPF-specific N-terminal (BN) domain also contributes to the association with the MYST domain. BRPF1 contains the PZP domain, bromodomain, and PWWP domain for chromatin association. Unlike its paralogs BRPF2 and BRPF3, BRPF1 has an Sfp1-like C2H2 zinc finger (SZ). NLS, nuclear localization signal; H1-like, histone H1–like domain; PZP, PHD–zinc knuckle–PHD; bromo, bromodomain; PWWP, Pro-Trp-Trp-Pro containing domain; SM, serine/methionine-rich (*8*, *23*). (**B**) BRPF1 promotes H3K23 propionylation. KAT6A was expressed in HEK293 cells as a FLAG-tagged fusion protein along with HA-tagged BRPF1, ING5, and MEAF6 as indicated. Affinity-purified proteins were used for acylation of HeLa oligonucleosomes in the presence of the respective acyl-CoA. Immunoblotting with antibodies recognizing histone H3 and its acylated forms was used to detect acylation states as indicated. See fig. S2A for immunoblotting analysis of the soluble extracts. Signals detected by the anti-H3K23cr and anti-H3K23bu antibodies need to be interpreted with caution due to cross-reactivity to H3K23ac and/or H3K23pr (see fig. S1B). (**C**) The H3K23 propionyltransferase activity is intrinsic to the MYST domain of KAT6A. Complex preparation and assays were performed as in (B) to compare KAT6A with its mutants. Recombinant mononucleosomes were used as substrate. See fig. S2B for immunoblotting analysis of the soluble extracts. Asterisks in (B) and (C) denote degraded products; the degradation varies from experiment to experiment. (**D**) Same as in (B) but ING4 and ING5 were compared. See fig. S2C for immunoblotting analysis of the soluble extracts. (**E**) Comparison of KAT6B fragments. Complex preparation and assays were performed as in (B) with the recombinant mononucleosome substrate, but KAT6B fragments were analyzed. Full-length KAT6B was difficult to express (*21*).

Downloaded from http://advances.sciencemag.org/ on February 12, 2020

and explore therapeutic strategies with histone deacetylase (HDAC) inhibitors and propionic acid.

RESULTS

Tetrameric BRPF1-KAT6 complexes propionylate histone H3K23 in vitro

KAT6A and KAT6B are paralogous and form tetrameric complexes with BRPF1, ING4 (or ING5), and MEAF6 (Fig. 1A) (*20*, *21*). To investigate whether the complexes propionylate H3K23, we carried out histone acylation assays with nucleosomes as the substrates. For this, KAT6A was expressed in human embryonic kidney (HEK) 293 cells as a FLAG-tagged fusion protein along with hemagglutinin (HA)–tagged BRPF1, ING5, and MEAF6, according to published procedures (*12*, *21*). Soluble extracts were prepared for affinity purification on anti-FLAG agarose. After stringent washing with a buffer containing 0.6 M KCl, bound proteins were eluted and used for acylation of HeLa oligonucleosomes [i.e., digested and purified from HeLa cell chromatin (*12*, *21*)] in the presence of acyl–coenzyme A (CoA) (e.g., acetyl- and propionyl-CoA for acetylation and propionylation, respectively; fig. S1A). The purified complexes were confirmed by immunoblotting analysis with anti-FLAG and anti-HA antibodies (fig. S1A, bottom two panels), whereas affinity-purified antibodies specific to histone H3 and its acylated forms were used to detect histone H3 or its H3K23 acylation, respectively. The acylation-specific antibodies specifically recognized H3K23 (fig. S1A, top five panels). Compared to H3K23 acetylation, endogenous H3K23 propionylation was low in HEK293 cells (fig. S1B, lanes 1 to 3). Notably, the anti-H3K23pr antibody was highly specific (fig. S1B).

As previously reported (*12*), when acetyl-CoA was used as the coenzyme, KAT6A acetylated H3K23 in HeLa oligonucleosomes, and BRPF1 stimulated this modification (Fig. 1B, top two panels). When propionyl-CoA was used as the coenzyme, KAT6A propionylated H3K23, and BRPF1 stimulated this new modification (Fig. 1B, panel 3 from the top). Mass spectrometry uncovered H3K23 crotonylation (cr) and H3K23 butyrylation (bu) (*2*, *3*). We then analyzed these two modifications (Fig. 1B, panels 4 and 5 from the top), but the antibodies cross-reacted with H3K23 acetylation and/or propionylation (fig. S1B, bottom two panels). Thus, we focused mainly on H3K23 propionylation for this study.

HeLa oligonucleosomes contain endogenous modifications (Fig. 1B, lane 1), so we analyzed the activity of the KAT6A complexes in acylation of recombinant mononucleosomes. As with HeLa oligonucleosomes, KAT6A acetylated or propionylated H3K23 in recombinant mononucleosomes, and BRPF1 stimulated these modifications (Fig. 1C, lanes 1 to 3). Because of no basal acylation in recombinant mononucleosomes (Fig. 1C, lane 1), the activities detected with KAT6A and its complexes were much more robust than those observed in the same assays with HeLa oligonucleosomes (compare Fig. 1, B and C, lanes 1 to 3). The MYST domain (Fig. 1A, bottom) was active in catalyzing this modification but less efficient than full-length KAT6A (Fig. 1C, lanes 3 and 4), whereas the N-MYST fragment (Fig. 1A, bottom) was more efficient than the MYST domain alone (Fig. 1C, lanes 4 and 5). To investigate whether the observed activity is intrinsic to this domain, we engineered and analyzed the MYST domain containing arginine substitution of Lys604, whose equivalent residues have been identified as autoacetylation sites essential for acetyltransferase activities of other MYST proteins (*37*). As shown in Fig. 1C (lanes 4 and 6), this mutant was inactive in promoting H3K23 acetylation or propionylation, thereby highlighting the critical importance of Lys604 and supporting that the observed activities are intrinsic to the MYST domain. Together, these results indicate that KAT6A propionylates H3K23 through the MYST domain in vitro.

During the analysis of the soluble extracts, we noticed, as reported previously (*12*), that with full-length KAT6A, BRPF1 promoted the expression of ING5 and MEAF6 (fig. S2A), perhaps due to the scaffold function of BRPF1 (Fig. 1A). This effect was similar with the N-MYST fragment (fig. S2B, lane 5) but much less evident with the MYST domain or its K604R mutant (lanes 4 and 6), suggesting that the N-terminal domain of KAT6A synergizes with BRPF1 in promoting the expression of ING5 and MEAF6.

It was reported previously that ING4 also copurified with KAT6A (*20*). In agreement with this, like ING5, ING4 formed tetrameric complex with the MYST domain of KAT6A, BRPF1, and MEAF6 (Fig. 1D, bottom two panels, and fig. S2C). Moreover, the ING4 complex was as active as the ING5 complex in H3K23 acylation (Fig. 1D, top three panels). Thus, ING4 and ING5 form similar H3K23 propionyltransferase complexes.

KAT6A is paralogous to KAT6B (Fig. 1A), so we investigated whether KAT6B also propionylates H3K23. For this, we analyzed two fragments containing the MYST domain of KAT6B (Fig. 1A, bottom). This MYST domain also efficiently propionylated recombinant mononucleosomes (Fig. 1E, lanes 1 and 2). The N-MYST fragment appeared to be more efficient than the MYST domain (Fig. 1E, compare lanes 2 and 3), indicating that the N-terminal part of KAT6B stimulates the enzymatic activity. This is similar to what was observed with the N-MYST fragment of KAT6A (Fig. 1C, lanes 4 and 5). As illustrated in Fig. 1A, the N-MYST fragment of KAT6A or KAT6B corresponds to the portion of leukemic fusion proteins resulting from leukemia-associated chromosomal translocations (*23*, *38*). These results suggest that the translocations do not affect acyltransferase activity of KAT6A or KAT6B.

Deletion of mouse *Brpf1* or *Kat6a* diminishes H3K23 propionylation in vivo

We next investigated whether the BRPF1-KAT6 complexes are histone H3K23 propionyltransferases in vivo. Deletion of mouse *Brpf1* markedly reduces H3K23 acetylation (*11*, *12*). By analogy, we hypothesized that *Brpf1* deletion has similar effects on H3K23 propionylation. To test this, we first carried out immunoblotting to detect histone H3 acylation in protein extracts from control and *Brpf1*$^{-/-}$ mouse embryonic fibroblasts (MEFs) (*39*). As previously reported (*11*, *12*), H3K23 acetylation was abolished in *Brpf1*$^{-/-}$ MEFs (Fig. 2A). H3K23 propionylation was undetectable in these mutant cells (Fig. 2A). By contrast, acetylation or propionylation at H3K9 (or H3K14) was not affected (Fig. 2A). The H3K23 propionylation deficiency was also observed in *Brpf1*$^{-/-}$ embryos (Fig. 2B). Moreover, immunofluorescence microscopy detected marked reduction of H3K23 propionylation in *Brpf1*$^{-/-}$ MEFs (Fig. 2C). Notably, the H3K23 propionylation level was more robust in mouse embryos than various cultured cells (fig. S3A). Thus, BRPF1 is critical for H3K23 propionylation in MEFs and embryos, supporting its relevance in vivo.

Brpf1 deletion also abrogated signals detected by the anti-H3K23cr and anti-H3K23bu antibodies in MEFs and embryos (Fig. 2, A and B), but this may be, in part, due to cross-reactivity with H3K23ac and H3K23pr (fig. S1B). We also analyzed total histone H3 acylation using anti-propionyllysine and anti-crotonyllysine antibodies. Both detected H3 acylation in wild-type and *Brpf1*$^{-/-}$ MEF extracts (fig. S3, B and C). Coimmunoprecipitation revealed that the anti-propionyllysine antibody

Downloaded from http://advances.sciencemag.org/ on February 12, 2020

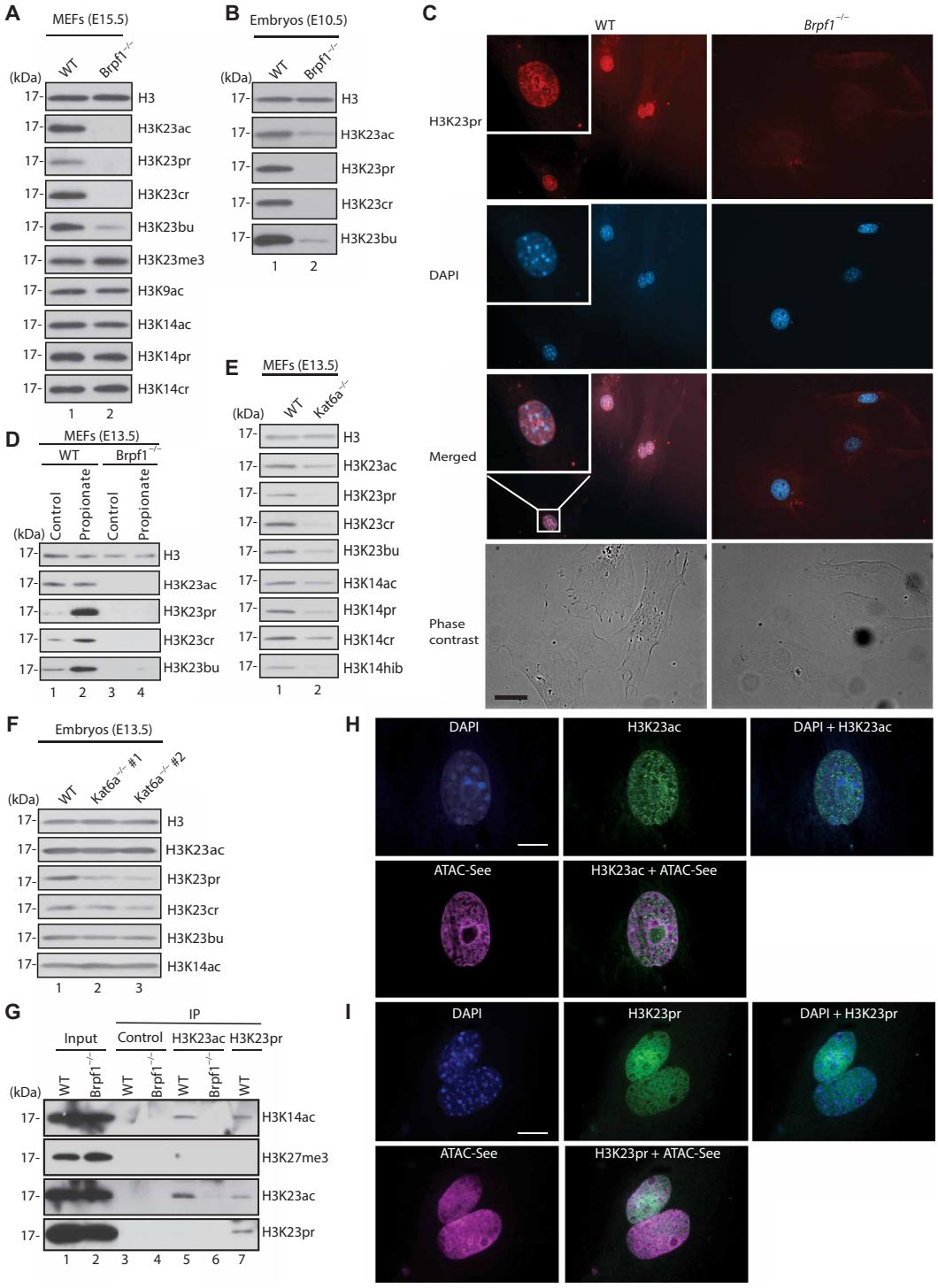

Fig. 2. *Brpf1* inactivation impairs histone H3K23 acylation in mouse fibroblasts and embryos. (**A**) Immunoblotting to detect histone H3 acylation in extracts from control and *Brpf1*$^{-/-}$ MEFs. The fibroblasts were prepared from control and tamoxifen-inducible *Brpf1* knockout embryos at E15.5 (*39*). (**B**) Immunoblotting to detect histone H3 acylation in extracts from wild-type and *Brpf1*$^{-/-}$ embryos at E10.5. (**C**) Immunofluorescence microscopic analysis of histone H3 propionylation in control and *Brpf1*$^{-/-}$ MEFs (E13.5). Scale bar, 20 μm. (**D**) Immunoblotting analysis to detect histone H3 acetylation and propionylation in extracts from control and *Brpf1*$^{-/-}$ MEFs (E13.5) cultured in the MEF medium supplemented with or without 10 mM sodium propionate for 24 hours. (**E**) Histone H3 acylation in extracts from control and *Kat6a*$^{-/-}$ MEFs. The fibroblasts were prepared from control and *Kat6a*$^{-/-}$ embryos at E13.5. (**F**) Histone H3 acylation in extracts from wild-type and *Kat6a*$^{-/-}$ embryos at E13.5. (**G**) Association of H3K23ac and H3K23pr with active chromatin. Soluble extracts from E13.5 wild-type (WT) and *Brpf1*$^{-/-}$ MEFs (lanes 1 and 2) were used for immunoprecipitation (IP) with control immunoglobulin G (IgG) (lanes 3 and 4), anti-H3K23ac antibody (lanes 5 and 6), or anti-H3K23pr antibody (lane 7). Immunoblotting was carried out with the antibodies specific to the histone marks indicated at the right. (**H** and **I**) Active chromatin of E13.5 wild-type MEFs was labeled with ATAC-See before immunofluorescence microscopy with the anti-H3K23ac (H) or anti-H3K23pr (I) antibody. Scale bars, 20 μm.

Downloaded from http://advances.sciencemag.org/ on February 12, 2020

recognizes histone H3 (fig. S3D). Thus, BRPF1 is not critical for total H3 acylation in vivo.

An interesting question is how H3K23 propionylation is regulated. One possibility is through propionyl-CoA. Because propionate CoA-transferase converts propionate and acetyl-CoA to propionyl-CoA, we treated MEFs with sodium propionate and analyzed the effect on H3K23 propionylation. As shown in Fig. 2D (lanes 1 and 2), this treatment enhanced H3K23 propionylation but not acetylation, highlighting their differential responses to different environmental conditions. The enhancement of propionylation in response to propionate treatment was abolished in *Brpf1*$^{-/-}$ MEFs (lanes 3 and 4), further supporting that *Brpf1* is required for H3K23 propionylation in vivo.

As BRPF1 activates KAT6A and KAT6B for H3K23 acylation in vitro (Fig. 1), we then examined histone H3 acylation in protein extracts from control and *Kat6a*$^{-/-}$ MEFs. As shown in Fig. 2E, H3K23 acetylation was reduced to about 30 to 50%, whereas H3K23 propionylation was barely detectable in *Kat6a*$^{-/-}$ MEFs (Fig. 2E). Moreover, in *Kat6a*$^{-/-}$ embryos, H3K23 acetylation was not affected, whereas H3K23 propionylation was reduced markedly (Fig. 2F). Residual H3K23 propionylation in mutant MEFs or embryos is likely due to *Kat6b*. These results support the view that KAT6A contributes substantially to H3K23 propionylation in vivo.

To determine functional consequences of H3K23ac and H3K23pr, we investigated whether they are associated with active chromatin. For this, we performed coimmunoprecipitation using the anti-H3K23ac or anti-H3K23pr antibody for immunoblotting with antibodies recognizing active and repressive chromatin marks. The anti-H3K23ac and anti-H3K23pr antibodies coimmunoprecipitated histone H3K14ac (an active chromatin mark) from wild-type MEF extracts (Fig. 2G, top, lanes 1, 3, 5, and 7). The former antibody failed to do so with *Brpf1*$^{-/-}$ MEF extracts (lanes 2, 4, and 6), indicating that BRPF1-promoted H3K23 acetylation is required for coimmunoprecipitation of histone H3K14ac. In contrast, neither antibody coimmunoprecipitated histone H3K27me3 (a repressive chromatin mark) from either wild-type or mutant MEF extracts (Fig. 2G), supporting the association of H3K23ac and H3K23pr with active but not repressive chromatin.

To substantiate the association with active chromatin, we also analyzed the subnuclear distribution of the modifications at the single-cell level. For this, active chromatin was labeled with ATAC-See, a recently developed technique to link oligonucleotide-coupled fluorophore covalently to active chromatin in situ (*40*). Then, H3K23 acylation was detected via fluorescence microscopy. H3K23ac- or H3K23pr-specific fluorescence signals were associated with chromatin labeled by ATAC-See in wild-type E13.5 (embryonic day 13.5) MEFs (Fig. 2, H and I). Moreover, similar results were obtained with sections prepared from wild-type mouse embryos (fig. S4, A and B). One noticeable difference between these two modifications was that propionylation, but not acetylation, was strong in the cerebrocortical neuroepithelium, highlighting the potential importance of H3K23 propionylation in cerebral development at the embryonic stage.

BRPF1 variants in 12 new cases of syndromic intellectual disability

Having established the BRPF1-KAT6 complexes as H3K23 propionyltransferases in vitro (Fig. 1) and in mice (Fig. 2), we then investigated the clinical relevance of these findings. We and others have reported 28 clinical cases of syndromic intellectual disability due to de novo or inherited *BRPF1* variants (*12*, *33*–*35*). We have now identified 12 previously unreported cases (Fig. 3A and table S1), thus bringing the total to 40. These cases are mainly from North America and Europe, where exome sequencing has been routinely used for clinical diagnosis of rare developmental disorders. As shown in table S1, most of the newly identified 12 individuals share key clinical features with those reported cases (*12*, *33*), including general developmental delay and gross/fine motor delay. Many showed intellectual disability and had language delay (table S1). Facial and eye dysmorphisms (e.g., blepharophimosis and ptosis) are common clinical features, with some individuals having vision problems (Fig. 3B, fig. S4C, and table S1). Hand and foot anomalies were also observed (Fig. 3C and table S1). Some individuals had ear and mouth anomalies (table S1). Hypotonia was observed in five cases (table S1). A subset exhibited electroencephalogram (EEG) abnormalities and behavioral issues, including attention deficit hyperactivity disorder (table S1). Related to intellectual disability and language delay, magnetic resonance imaging (MRI) analysis detected brain abnormalities (Fig. 3D and table S1), e.g., dysmorphism or thinning of the corpus callosum in individuals P7 and P12 (table S1). One individual displayed cardiac anomalies (P10; table S1). Albeit different, cardiac anomalies were also observed in the previously described individual with the Trp315Leufs*26 variant (Fig. 3E) (*12*). Although not universally evaluated in this and the previous cohort, cardiac anomalies in these two cases indicate a less common clinical finding.

The variant c.227C>T in individual P1 (table S1) was inherited from an asymptomatic father, suggesting incomplete genetic penetrance. This variant is present in P1's 1-year-old brother, who has not yet undergone developmental assessment (table S1). Despite language delay, individual P2 displays typical cognitive functioning (table S1). Moreover, the c.883_884del variant in individual P4 was inherited from her mother (individual P5), who exhibits few clinical features; P4's intelligence quotient (IQ) is within the normal range (table S1). These new findings support variable clinical expressivity. Related to this, a new study described three brothers who inherited the Gln186* variant from their mother (*35*). The mother is 61 years old, with self-perceived normal cognitive function, whereas her three sons are all affected (*35*). Genetic background and environmental influence may contribute to incomplete penetrance and variable expressivity.

In the 12 cases identified here (Fig. 3A and table S1), there are 11 different *BRPF1* variants. One of them is shared by a girl and her mother (Fig. 3A, c.883_884del, individuals P4 and P5). Moreover, the variant in individual P11 (Fig. 3A, c.2497C>T) is identical to a previously described one (*33*), so there are only 10 new variants. Six of them lead to C-terminal truncations expected to inactivate *BRPF1* (Fig. 3A). For similar truncations, we have established that the variant transcripts escape nonsense-mediated mRNA decay (*12*). Some truncation variants, such as Gln96* and Asp187Glyfs*29 (Fig. 3A), may display poor expression, as we have shown for the Glu121Glyfs*2 variant (Fig. 4A) (*12*). Both Gln96* and Asp187Glyfs*29 also lack the domains for KAT6A/KAT6B interaction (Fig. 3A). Met295Valfs*17 and Thr434Profs*61 contain these domains but lack an intact PZP (PHD–zinc knuckle–PHD) domain for nucleosome binding (Fig. 3A). This domain is critical for BRPF1 to promote nucleosomal H3K23 acetylation by KAT6A (*12*). Both Glu474Glyfs*3 and Tyr543Thrfs*6 lack intact ECP-II required for ING5/MEAF6 binding (Fig. 3A). Thus, the six new truncating variants are likely pathogenic.

Downloaded from http://advances.sciencemag.org/ on February 12, 2020

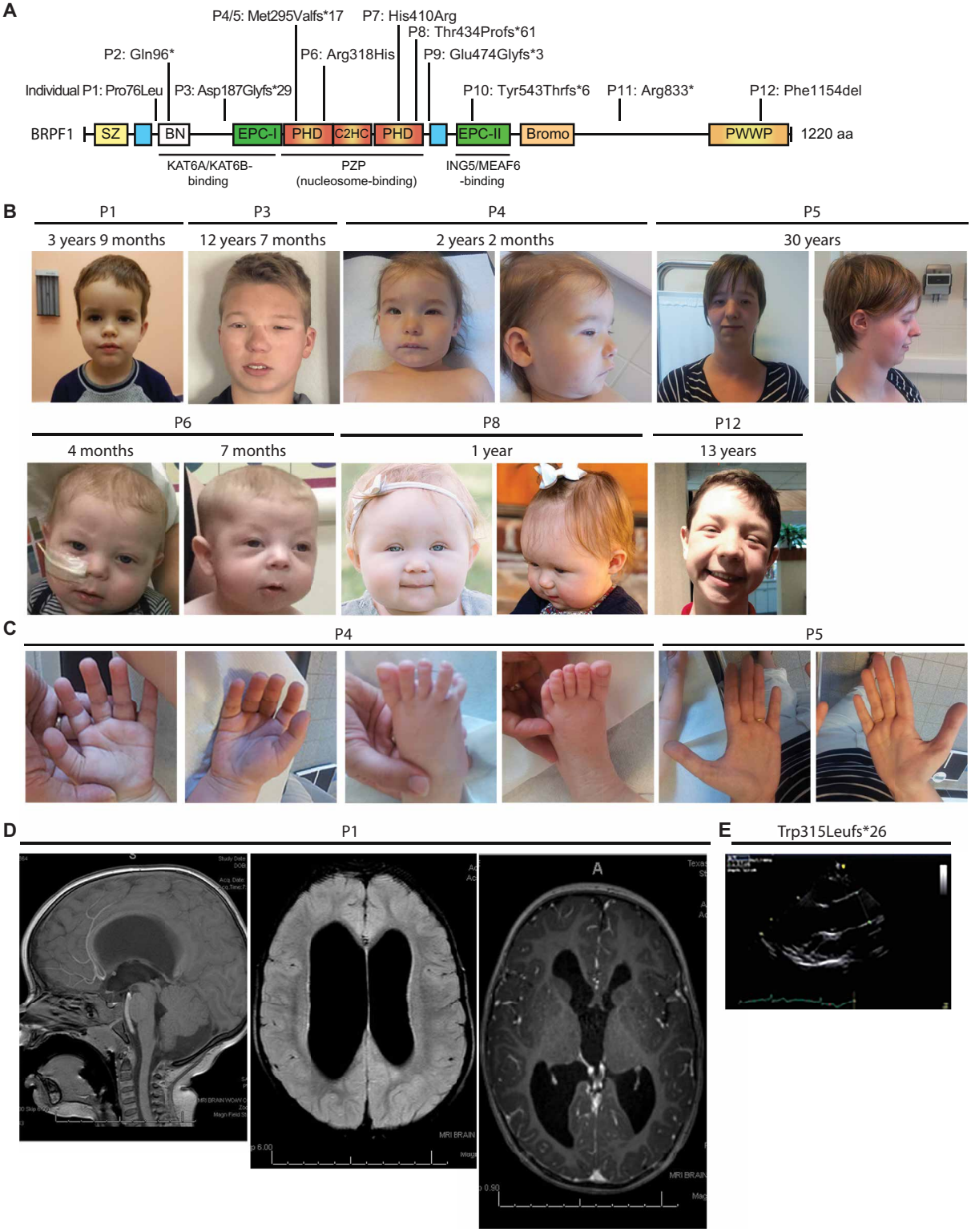

Fig. 3. Clinical characteristics of newly identified individuals with *BRPF1* variants. (**A**) Schematic representation of variants identified in 12 newly identified individuals with syndromic intellectual disability. See Fig. 1A for domain nomenclature. (**B**) Facial features of seven individuals with heterozygous *BRPF1* mutations. The ages when the photos were taken are indicated. See fig. S4C for additional photos. (**C**) Hand and foot photos of individuals P4 and P5. (**D**) Brain MRI images of individual P1. (**E**) Echocardiographic image of dilated ascending aorta in a previously reported case (*12*). Photo credit: The authors confirm that permissions were received to use all images, but to protect patient identity, photographer names remain anonymous.

Downloaded from http://advances.sciencemag.org/ on February 12, 2020

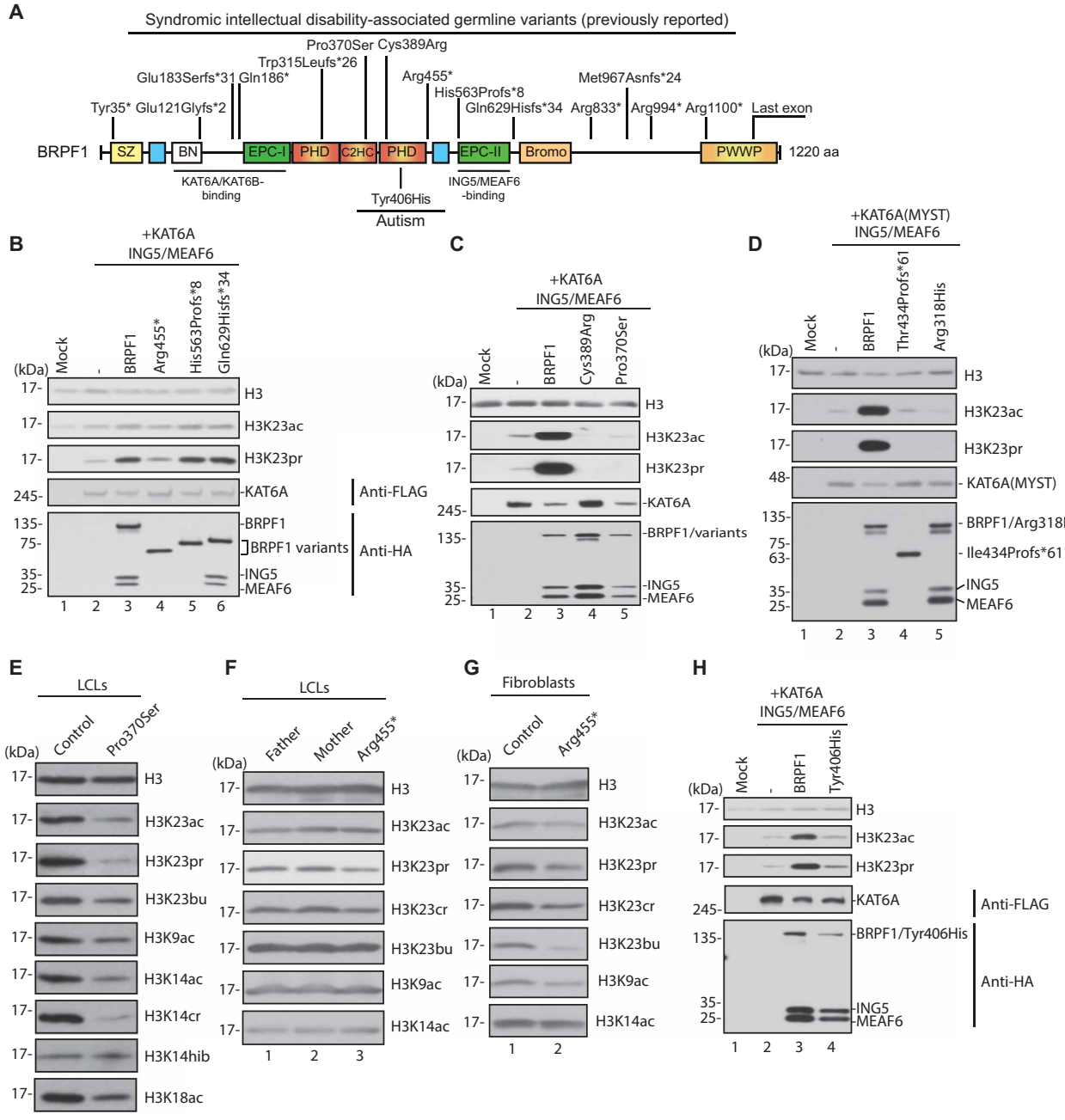

Fig. 4. Functional impact of *BRPF1* variants associated with neurodevelopmental disorders. (**A**) Cartoon representation of variants previously identified in 29 individuals with syndromic intellectual disability (*12*, *33*–*36*) or autism (*43*). See Fig. 1A for domain nomenclature. (**B**) Nucleosomal acylation assays. HeLa oligonucleosomes were used for acylation by the affinity-purified wild-type and mutant complexes. The complexes were prepared for assays as in Fig. 1B. See fig. S2D for immunoblotting analysis of the soluble extracts. (**C**) Nucleosomal histone acylation assays. Recombinant mononucleosomes were used for acylation by the affinity-purified wild-type and mutant complexes. (**D**) Assays were carried out similarly as in (C), and the MYST domain of KAT6A was used. See fig. S2E for immunoblotting analysis of the soluble extracts. (**E**) Immunoblotting to detect histone H3 acylation in extracts from control and the Pro370Ser LCLs. (**F**) Immunoblotting to detect histone H3 acylation in protein extracts from the control and Arg455* LCLs. (**G**) Immunoblotting to detect histone H3 acylation in extracts from the control and Arg455* fibroblasts. (**H**) Assays were carried out similarly as in (C), but the Tyr406His variant was analyzed. See fig. S2F for immunoblotting analysis of the soluble extracts.

Among the remaining four new variants (Fig. 3A), three alter Pro76, Arg318, and His410, with the fourth generating in-frame deletion of Phe1154. These four residues are evolutionarily conserved from *Drosophila* to humans (figs. S5 and S6). His410 is a key zinc-chelating residue (figs. S5 and S7A), so His410Arg likely disrupts the PZP domain. Phe1154 is an integral part of the trimethyl-histone binding pocket of the PWWP (Pro-Trp-Trp-Pro) domain (Fig. 3A and fig. S7B) (*41*, *42*), so Phe1154del likely inactivates this domain. Pro76 is located at the N-terminal region, whereas Arg318 is within the first PHD of the PZP domain (Fig. 3A). The functional impact of Pro76Leu and Arg318His is not obvious and thus needs further experimental validation.

Downloaded from http://advances.sciencemag.org/ on February 12, 2020

Developmental disorder-associated *BRPF1* mutations diminish H3K23 acylation

Because *BRPF1* variants were found to cause H3K23 acetylation deficiency (*12*, *33*), we asked whether H3K23 propionylation is also impaired (Fig. 3A). To assess this, we expressed and affinity-purified tetrameric KAT6A complexes containing wild-type or mutant BRPF1 proteins for histone acylation assays. As noticed previously (*12*), Gln629Hisfs*34, but not Arg455* or His563Profs*8, promoted expression of ING5 and MEAF6 (fig. S2D, lanes 1 to 5). This is because the latter two do not contain EPC-II (enhancer of polycomb II) essential for ING5/MEAF6 binding (Fig. 4A). ING5 and MEAF6 did not copurify with these two variants (Fig. 4B, bottom two panels, lanes 4 and 5, and fig. S2D). Unlike Arg455*, both His563Profs*8 and Gln629Hisfs*34 stimulated H3K23 acetylation or propionylation by KAT6A (Fig. 4B, top three panels). The observed activity of His563Profs*8 suggests that ING5/MEAF6 binding is dispensable for BRPF1 to stimulate acylation by KAT6A. As previously reported (*12*), the loss of the PWWP domain in Gln629Hisfs*34 (Fig. 4A) may affect histone methylation–based genome targeting in vivo.

We also analyzed the four missense variants (Pro76Leu, Arg318His, Pro370Ser, and Cys389Arg). Among them, Pro370Ser is defective for stimulating H3K23 acetylation by KAT6A (*12*). Like this mutant, Cys389Arg was also inactive in stimulating H3K23 acetylation (Fig. 4C, top two panels). Neither variant stimulated H3K23 propionylation by KAT6A (Fig. 4C, middle). As shown in Fig. 4D (bottom two panels) and fig. S2E, Arg318His formed a tetrameric complex normally with the MYST domain of KAT6A, ING5, and MEAF6, but Thr434Profs*61 did not interact with ING5 and MEAF6. This is expected as this variant lacks EPC-II required for ING5/MEAF6 binding (Fig. 3A). Neither Thr434Profs*61 nor Arg318His stimulated H3K23 acetylation or propionylation by the MYST domain of KAT6A (Fig. 4D, top three panels).

The Pro76Leu variant was normally expressed and promoted the expression of ING5 and MEAF6 as wild-type BRPF1 (fig. S7C). Moreover, similar to wild-type BRPF1, this variant stimulated H3K23 acylation by KAT6A (fig. S7D). As Pro76 is located at a serine-rich region (fig. S5), this variant may be affected in vivo in terms of regulation by phosphorylation. Clinical features such as macrocephaly also make this case stand out from the cohort (table S1). Further studies are needed to clarify this variant's relationship to neurodevelopmental disorders and assess if it is affected differently from other variants in vivo. Thus, except for Pro76Leu, the *BRPF1* variants are inactive in promoting H3K23 acylation by KAT6A.

To establish the in vivo relevance, we analyzed H3K23 propionylation in cells from individuals with *BRPF1* variants. As shown in Fig. 4E, this modification decreased in the lymphoblastoid cells (LCLs) prepared from the individual harboring the Pro370Ser variant. Moreover, a similar albeit less marked deficiency was also observed in the LCLs and fibroblasts from the individual with the Arg455* variant (Fig. 4, F and G). While *BRPF1* variants identified so far are distributed across the entire protein (Figs. 3A and 4A) (*12*, *33*), most of the *KAT6A* and *KAT6B* variants associated with syndromic intellectual disability delete the C-terminal part but leave the MYST domain intact (fig. S8, A and C) (*24*–*31*). Nonsense-mediated mRNA decay does not appear to affect transcripts with truncating mutations because most of them are located within the last large coding exon (*24*–*30*), so many *KAT6A* or *KAT6B* variants are not expected to alter H3K23 acetylation and propionylation. Neither was affected in cells with *KAT6A* or *KAT6B* variants (fig. S8, B and D). Thus, these variants do not impair H3K23 acylation.

A *BRPF1* Tyr406His variant was identified in an autistic individual (*43*), but the pathogenicity remains elusive. Tyr406 is highly conserved from *Caenorhabditis elegans* to humans (fig. S5), so we examined the activity of this variant. This variant was well expressed (fig. S2F), but it did not copurify well with KAT6A (Fig. 4H, bottom two panels). Moreover, the variant complex was also less active than the wild type in promoting H3K23 acetylation and propionylation by KAT6A (top three panels), supporting the pathogenicity of the corresponding variant. These results indicate that BRPF1 dysfunction also contributes to autism spectrum disorder (*43*), further attesting to phenotypic variation associated with *BRPF1* variants and suggesting that they may be broadly associated with neurodevelopmental disorders.

Somatic cancer mutations perturb H3K23 acylation via different mechanisms

In addition to germline mutations in individuals with neurodevelopmental disorders (Figs. 3A and 4A), somatic *BRPF1* mutations have been identified in medulloblastoma, leukemia, and other types of cancer (Fig. 5A and figs. S5 and S9) (*23*, *44*, *45*). According to The Cancer Genome Atlas datasets, there are 211 cases with 236 *BRPF1* mutations, corresponding to ~2% of the 10,240 cancer cases analyzed (fig. S9). Like those germline variants identified in individuals with neurodevelopmental disorders (Figs. 3A and 4A), these somatic mutations primarily comprise two groups: truncating and missense. According to published reports (*12*, *33*) and the results in Fig. 4, the truncating somatic mutations are expected to inactivate the mutant alleles.

Among the missense mutants, Pro20Leu, Arg29Cys, and Ser36Ile alter an N-terminal region with no known function (Fig. 5A and fig. S5). This region is absent in the BRPF1 paralogs BRPF2 and BRPF3 but highly conserved in BRPF1 proteins from *Drosophila* to humans (fig. S5). BLAST (Basic Local Alignment Search Tool) search revealed high similarity to a C2H2 zinc finger shared by a group of proteins, including the yeast transcription factor Sfp1, so we referred to this unique N-terminal region as the Sfp1-like zinc finger (SZ) domain. Pro20 is highly conserved among this group of proteins (Fig. 5B) and invariant among BRPF1 proteins from *Drosophila* to humans (fig. S5), suggesting the importance of this residue. As shown in fig. S2G (lanes 1 to 3), this mutant was much more difficult to express than wild-type BRPF1 and also failed to promote expression of ING5 and MEAF6. Moreover, this mutant formed a suboptimal tetrameric complex with KAT6A, ING5, and MEAF6 (Fig. 5C, bottom two panels). The mutant barely stimulated H3K23 acetylation or propionylation by KAT6A (Fig. 5C, top three panels, compare lanes 2 and 4). Thus, the mutation affects expression, complex formation, and enzymatic activity.

One hotspot mutation is recurrent in six cancer cases and encodes Arg66Cys (fig. S9). This residue is part of a putative nuclear localization signal, NLS1 (Fig. 1A and fig. S5), so the mutant may affect the function of this NLS. Moreover, three other cancer-associated mutants (Arg59His, Arg59Cys, and Gln67Pro) alter Arg59 and Gln67, both of which are part of NLS1. We thus analyzed the function of this NLS. As shown in Fig. 5D, a fragment (residues 1 to 57) containing the SZ domain of BRPF1 was localized to the nucleus and cytoplasm, with some enrichment in the former. Unlike the full-length BRPF1, coexpression of KAT6A, with or without ING5 and MEAF6, did not affect this subcellular distribution. Compared to the mutant 1-57, the fragment containing the N-terminal 71 residues was more enriched in the nucleus (Fig. 5D), indicating that NLS1 is a functional NLS. Thus, Arg66Cys, Arg59His, Arg59Cys, and Gln67Pro likely affect the function of NLS1.

Downloaded from http://advances.sciencemag.org/ on February 12, 2020

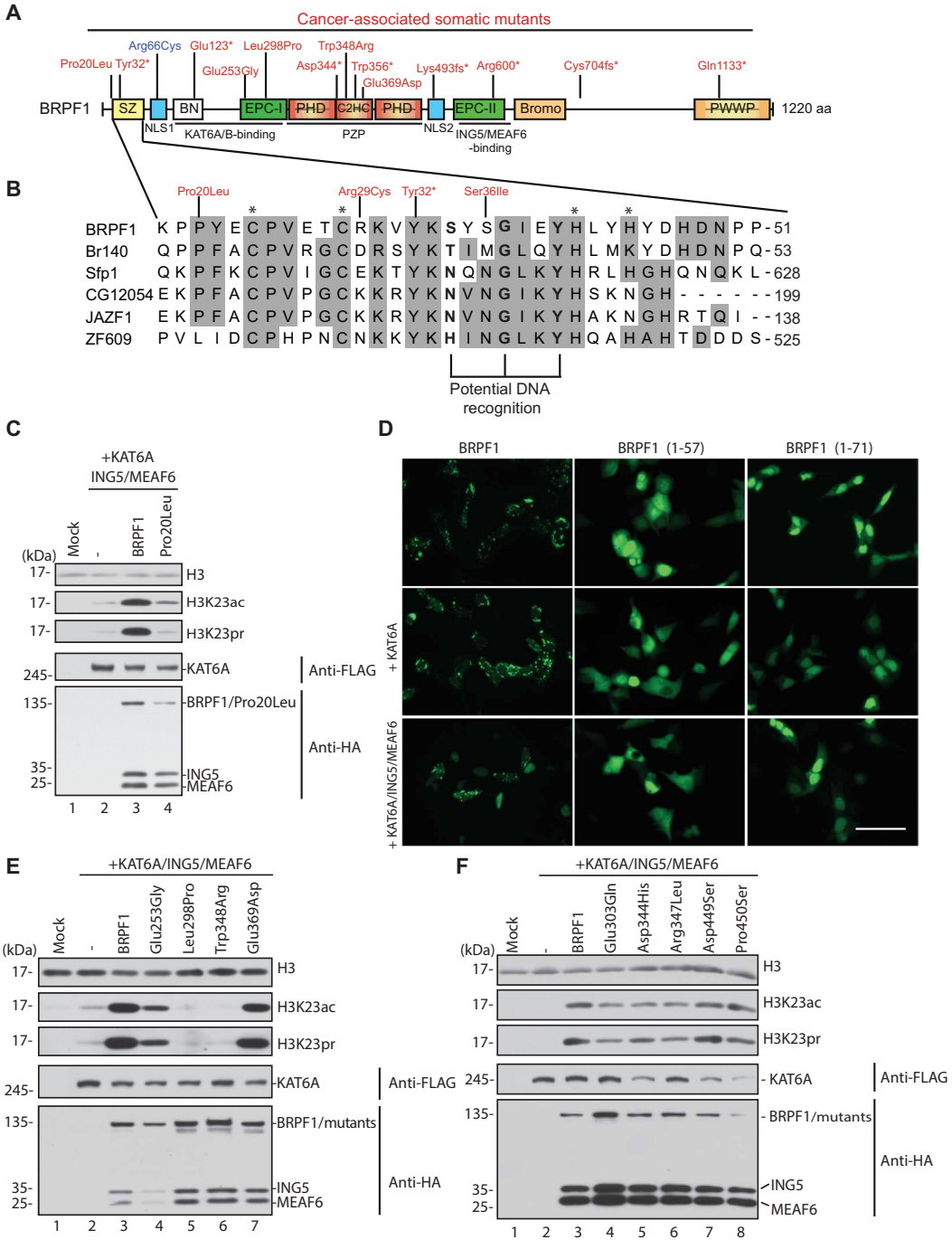

Fig. 5. Functional impact of somatic *BRPF1* mutations from cancer. (**A**) Cartoon representation of somatic mutants identified in cancer. While five mutations are missense and produce Pro20Leu, Glu253Gly, Leu298Pro, Trp348Arg, and Glu369Asp, the rest are nonsense or cause reading frameshift, resulting in C-terminal truncation. According to the published report on other truncation mutations of *BRPF1* (*12*), these nonsense or frameshift mutations may not trigger nonsense-mediated mRNA decay. See Fig. 1A for domain nomenclature. (**B**) Sequence similarity among the C2H2 zinc fingers of BRPF1, the fly ortholog Br140, the yeast stress- and nutrient-sensing transcription factor Sfp1, the fly Sfp1-like protein CG12054, and the related human transcription factors JAZF1 and ZF609. The SZ of BRPF1 is similar to the first of two zinc fingers that Sfp1 has for DNA binding and homologous to the middle of three zinc fingers that JAZF1 uses to recognize DNA. The three key residues involved in known and potential DNA binding are highlighted in bold. (**C**) Nucleosomal acylation assays. Recombinant mononucleosomes were used for acylation by the affinity-purified wild-type and mutant complexes as in Fig. 1C. Acylation of histone H3 was detected with antibodies recognizing histone H3 and its acylated forms as indicated. See fig. S2G (lanes 1 to 3) for immunoblotting analysis of the soluble extracts. (**D**) Subcellular localization of wild-type BRPF1 and its N-terminal mutants 1-51 and 1-71. Mutant 1-51 contains the SZ, and mutant 1-71 has this finger along with adjacent NLS1. Expression plasmids for BRPF1 or its mutants were transiently expressed in HEK293 cells as green fluorescent protein (GFP) fusion proteins with or without coexpression of FLAG- or HA-tagged KAT6A, ING5, and MEAF6 as indicated. Live green fluorescence images were taken. Scale bar, 50 μm. (**E** and **F**) Same as (C) except different variants were compared to wild-type BRPF1. See fig. S2G (lane 4) for immunoblotting analysis of extracts from HEK293 cells expressing Glu253Gly.

Downloaded from http://advances.sciencemag.org/ on February 12, 2020

We then verified the activity of Glu253Gly, Leu298Pro, Trp348Arg, and Glu369Asp, all of which were identified in medulloblastoma (*44*). As illustrated in Fig. 5A, Glu253 and Leu298 are located at EPC-I required for KAT6A/B binding, whereas Trp348 and Glu369 are within the PZP domain important for nucleosome binding. Glu253Gly promoted expression of ING5 and MEAF6 (fig. S2G, compare lanes 1 and 2 with lane 4) but formed a suboptimal complex with KAT6A (Fig. 5E, bottom two panels, lanes 3 and 4). The interaction with ING5 and MEAF6 was also compromised (Fig. 5E, bottom, lanes 3 and 4, and fig. S2G, lanes 1, 2, and 4). This mutant was less active than wild-type BRPF1 in stimulating H3K23 acetylation and propionylation by KAT6A (Fig. 5E, top three panels, lanes 2 to 4). Unlike this mutant, Leu298Pro, Trp348Arg, and Glu369Asp all formed normal tetrameric complexes with KAT6A, ING5, and MEAF6 (Fig. 5E, bottom two panels, lanes 5 to 7). However, unlike Glu369Asp, neither Leu298Pro nor Trp348Arg stimulated H3K23 acetylation or propionylation by KAT6A (Fig. 5E, top three panels, lanes 5 to 7). Thus, Glu253Gly, Leu298Pro, and Trp348Arg, but not Glu369Asp, inactivated BRPF1. We also analyzed five other cancer-derived missense mutants that alter the PZP domain or its C-terminal region (Fig. 5F). Among them, Glu303Gln showed a modestly reduced activity in stimulating H3K23 acylation by KAT6A, whereas Asp344His, Arg347Leu, and the two other mutants were comparable to wild-type BRPF1 (Fig. 5F). Therefore, cancer-derived somatic *BRPF1* mutations exert variable effects on H3K23 acylation, reiterating that the impact of each mutation needs to be verified experimentally.

Pharmacological manipulation of histone H3K23 acylation

Having established deficient H3K23 acylation caused by *BRPF1* variants from individuals with syndromic intellectual disability (Fig. 4) (*12*, *33*) or by somatic mutants from cancer cells (Fig. 5), we tested potential means to reverse the deficiency. For this, we first investigated whether various HDAC inhibitors up-regulate H3K23 acylation. For this, we treated HEK293 cells with valproic acid (anti-epileptic drug with HDAC inhibitor activity), suberoylanilide hydroxamic acid (SAHA) (anti-lymphoma drug, also known as vorinostat), β-hydroxybutyrate (a common metabolite with HDAC inhibitor activity), trichostatin A (TSA; antifungal compound identified as the first specific HDAC inhibitor), and butyrate (nonspecific HDAC inhibitor and common end product from fermentation of dietary fiber by gut microbiota) (*46*, *47*). As shown in Fig. 6A, all these inhibitors except β-hydroxybutyrate up-regulated H3K23 acetylation and propionylation. We then tested *Brpf1*$^{-/-}$ MEFs. As shown in Fig. 6B, all five HDAC inhibitors corrected the deficiency in H3K23 acetylation and propionylation. We also tested LCLs from the individual harboring the Pro370Ser variant. As shown in Fig. 6C, all inhibitors except β-hydroxybutyrate enhanced H3K23 acetylation and propionylation. These results suggest potential means to rescue deficient H3K23 acylation.

These inhibitors target classical HDACs instead of sirtuins (*47*). In the classical family, HDAC1, HDAC2, and HDAC3 are major deacetylases for histone deacetylation (*47*). Thus, the above results suggest the involvement of these three deacetylases in H3K23 deacylation. Related to this, an HDAC3-specific inhibitor enhanced H3K23 acetylation in transformed cells (HEK293) and a breast cancer cell line (MCF7; Fig. 6D). These results suggest that HDAC3 contributes to H3K23 deacylation. Because an HDAC1/2-specific inhibitor also up-regulated H3K23 acetylation (*48*), multiple deacetylases may govern H3K23 deacylation.

Propionate treatment enhanced H3K23 propionylation in MEFs (Fig. 2D), suggesting another strategy to reverse the deficiency. We thus applied the treatment to LCLs derived from an individual with syndromic intellectual disability and the Pro370Ser variant (Fig. 4, A and C) (*12*). As shown for MEFs (Fig. 2D), propionate enhanced H3K23 propionylation in wild-type LCLs cells (Fig. 6E, middle two panels, lanes 1 and 3), supporting the view that H3K23 propionylation is subject to dynamic regulation by metabolic cues. The treatment also enhanced H3K23 propionylation in the patient-derived LCLs (middle two panels, lanes 2 and 4). The level was even higher than that in wild-type LCLs (compare lanes 1 and 4). Propionate is a common short-chain fatty acid (SCFA) produced from microbiotal fermentation of dietary fiber in the gut (*46*), suggesting that dietary modulation may be one potential means for modulating histone propionylation.

DISCUSSION

Histone propionylation has recently been identified via mass spectrometry (*3*), but it remains to be established what enzymes catalyze this novel acylation in vivo. The results presented here show unequivocally that BRPF1-KAT6 complexes are authentic histone H3K23 propionyltransferases in vitro and in vivo (Figs. 1, 2, and 6F). For the enzymatic assays carried out in vitro (Fig. 1, B and C), we used native and recombinant nucleosomes, rather than histone peptides. To establish the biological relevance, we analyzed mouse *Brpf1* disruption and human *BRPF1* variants (Figs. 2 to 4). *Brpf1* deletion obliterated H3K23 acylation in mouse embryos and fibroblasts (Fig. 2). *BRPF1* variants from individuals with neurodevelopmental disorders (Fig. 4) or from cancer cells (Fig. 5) impaired BRPF1 in activating KAT6A for H3K23 propionylation. We have also obtained evidence on potential means to manipulate this modification with two known drugs (valproic acid and vorinostat) (Fig. 6, A to C) or by treatment with propionate (Fig. 6E). Moreover, we demonstrated that propionate and butyrate, two common SCFAs produced from microbiota fermentation of dietary fiber (*46*), promote the modification through different mechanisms (Fig. 6G). Previous reports established that fly and mammalian KAT6 proteins are H3K23 acetyltransferases (*10*–*12*). Together with these reports, the current study supports that KAT6-BRPF1 complexes are dual-functional enzymes for H3K23 acetylation and propionylation.

Histone acetylation is mainly associated with chromatin assembly and gene activation (*1*). Chemically, propionylation is analogous to acetylation (*3*), so an important question is what functions this acetylation-like acylation has in vivo. We performed coimmunoprecipitation (Fig. 2G) and immunofluorescence microscopy (Fig. 2, H and I, and fig. S4, A and B) to investigate the association with active chromatin labeled by ATAC-See in situ (*40*). The results indicated that H3K23pr is associated with active chromatin. Related to this, H3K23pr fluorescence signals were not localized to heterochromatic nuclear foci heavily stained with 4′,6-diamidino-2-phenylindole (Fig. 2, C, H, and I). In flies, H3K14pr colocalizes with active genetic loci at the genome-wide level (*49*). Moreover, histone crotonylation is associated with transcriptional activation (*6*, *50*). Theoretically, H3K23pr is mutually exclusive with other acylation (such as acetylation) of the same residue. In future analysis of genome-wide association of H3K23pr, it shall be interesting to investigate how this mark is associated with active genetic loci and its genome-wide distribution is different from that of H3K23ac.

A puzzling question is why BRPF1-KAT6 complexes serve as dual-functional enzymes for H3K23 acetylation and propionylation.

Downloaded from http://advances.sciencemag.org/ on February 12, 2020

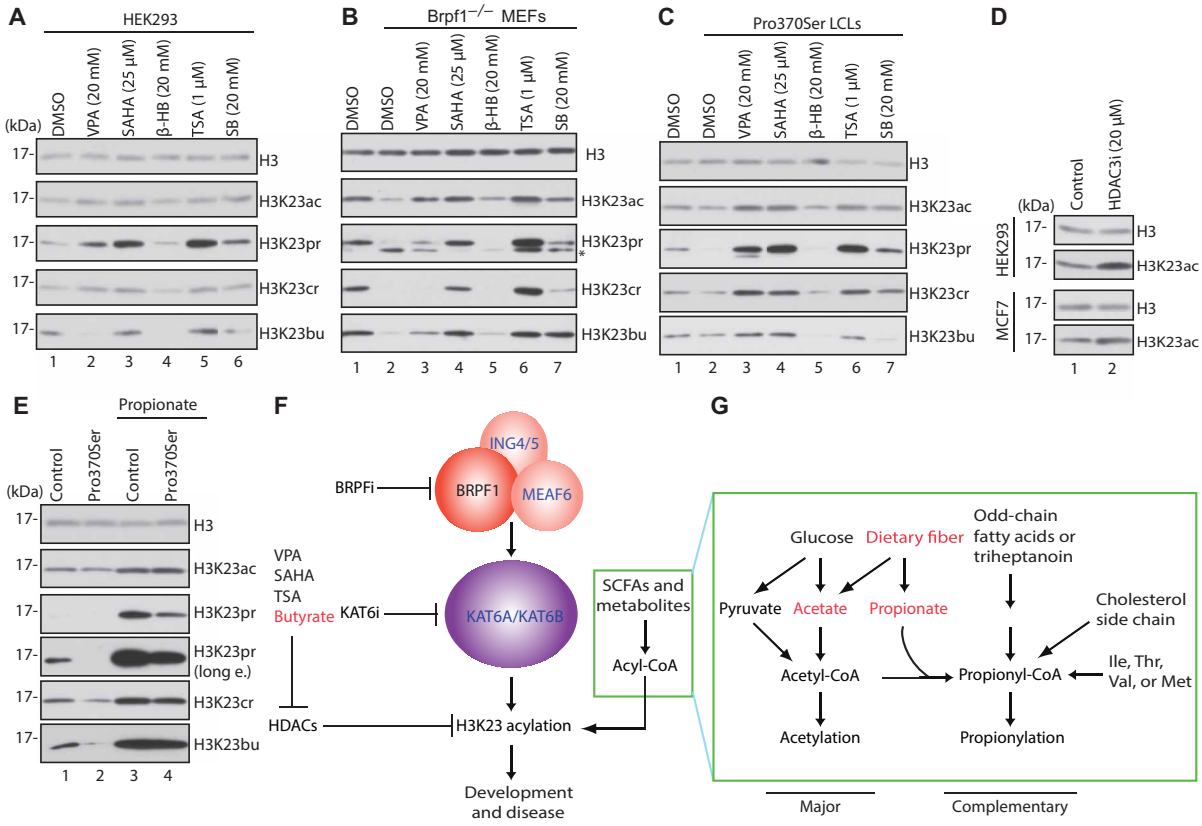

Fig. 6. Manipulation of histone H3K23 acylation with various compounds. (**A**) Up-regulated histone H3K23 acylation in HEK293 cells treated with the indicated HDAC inhibitor valproate (VPA), vorinostat (SAHA), β-hydroxybutyrate (β-HB), TSA, or sodium butyrate (SB) for 24 hours. DMSO, dimethyl sulfoxide. (**B**) Rescue of histone H3K23 acylation deficiency in *Brpf1*$^{-/-}$ MEFs by HDAC inhibitors. (**C**) Rescue of histone H3K23 acylation deficiency in patient-derived LCLs by HDAC inhibitors. For (A) to (C) and (E), results with the anti-H3K23cr and anti-H3K23bu antibodies need to be interpreted with caution due to cross-reactivity with H3K23ac and/or H3K23pr (fig. S1B). (**D**) Effect of an HDAC3-specific inhibitor. The indicated cells were treated with the inhibitor RGFP966 for 15 hours. (**E**) Rescue of histone H3K23 acylation deficiency in patient-derived LCLs by propionate. Control and patient-derived LCLs were cultured in a medium supplemented with or without 10 mM sodium propionate for 24 hours. For immunoblotting analysis with the anti-H3K23pr antibody, a long exposure (long e.) was also shown (panel 4 from the top). (**F**) Model explaining how BRPF1 acts through KAT6A and KAT6B for controlling histone H3K23 acylation and regulating developmental and pathological processes. HDAC inhibitors such as VPA, SAHA, TSA, and butyrate up-regulate acylation. These compounds offer therapeutic potential for the related diseases. Short-chain fatty acid (SCFAs) and other metabolites regulate acyl-CoA levels, thereby controlling H3K23 acylation. (**G**) Expanded version of the green box in (F) highlighting how various metabolites may differentially regulate acetylation and propionylation. For simplicity, only pyruvate and acetate are illustrated for events upstream from acetyl-CoA, a central player downstream from diverse metabolic pathways. On the basis of relative concentrations of acetyl-CoA and propionyl-CoA in vivo, we propose that acetylation plays a major role, whereas propionylation complements acetylation.

Although propionylation is chemically similar to acetylation, these two modifications are quite different at the metabolic level. One key difference lies at distinct acyl-CoA molecules needed as coenzymes. As shown in Fig. 6G, acetyl-CoA is downstream from the common metabolites pyruvate and acetate, whereas propionyl-CoA is controlled by propionate, as well as by metabolites from β-oxidation of odd-chain fatty acids and from metabolism of cholesterol and the amino acids Ile, Thr, Val, and Met. Moreover, triheptanoin, a drug in clinical trial for fatty acid oxidation disorders, contains three odd-carbon fatty acids (Fig. 6G). Activities of BRPF1-KAT6A/B complexes in acetylating and propionylating H3K23 in response to acetyl-CoA and propionyl-CoA, respectively, confer functional versatility under different metabolic conditions. Because some protein domains recognize acetylation and other acylation differently (*2*, *3*), H3K23 acetylation and propionylation may trigger distinct impact on transcriptomes. Because the acetyl-CoA concentration is much higher than propionyl-CoA in vivo (*51*), propionylation may function when and where the propionyl-CoA level increases to serve as a regulatory mechanism complementary to acetylation (Fig. 6G). The relative concentration of propionyl-CoA is higher in the liver than the heart, kidney, brain, and muscle (*51*), so the importance of propionylation may vary from tissue to tissue. In addition, H3K23pr is more abundant in mouse embryos than in cultured cells (fig. S3A), so propionylation may fluctuate as development progresses. Notably, the propionyl-CoA level is elevated in clinical cases of propionic acidemia, a recessive genetic disorder that is typically rare but quite prevalent in the Greenlandic Inuit population, Amish communities, the Middle East, and North Africa (*52*). The elevated propionic acid and propionyl-CoA levels in these cases could lead to hyperpropionylation (*53*).

Downloaded from http://advances.sciencemag.org/ on February 12, 2020

Acetate, propionate, and butyrate are the most common SCFAs produced from fermentation of dietary fiber by gut microbiota (*46*). These SCFAs are of direct importance to physiology and health of the host. Two signaling functions have been assigned to these SCFAs. All of them can function as G protein–coupled receptor agonists, whereas butyrate, but not acetylate or propionate, also acts as an HDAC inhibitor (*46*). As expected from its activity as an HDAC inhibitor, butyrate promoted H3K23 acetylation and propionylation (Fig. 6, A to C). Related to this, phenylbutyrate is used to treat urea cycle disorders. Propionate treatment stimulated H3K23 propionylation but not acetylation in MEFs (Fig. 2D) and patient cells (Fig. 6F). This is likely through propionyl-CoA (Fig. 6G). These results identify a third signaling function for SCFAs and link H3K23 propionylation to fermentation of dietary fiber by the intestinal microbiota.

As for pathological relevance, *KAT6A* and *KAT6B* are rearranged or amplified in leukemia and other cancers (*23*, *54*). Leukemia-associated chromosomal translocations tend to leave the MYST domains of KAT6A and KAT6B intact (Fig. 1A) (*23*, *38*). *KAT6A*, *KAT6B*, and *BRPF1* are also frequently amplified in some cancer types (fig. S9) (*23*). In these cases, unwanted acylation may be the culprit, so BRPF1 and KAT6 inhibitors (Fig. 6F) may be of therapeutic value due to their activity to mitigate elevated acylation. On the other hand, inactivating *BRPF1* mutations are associated with medulloblastoma and other cancer types (Fig. 5) (*44*, *45*). In these cases, up-regulation of H3K23 acylation by deacetylase inhibitors (Fig. 6) may be of therapeutic value. Thus, specific mutation-based strategies are needed for different genomic contexts.

KAT6A or *KAT6B* variants have been identified in ~300 individuals with neurodevelopmental disorders characteristic of intellectual disability (*24*–*32*). *BRPF1* variants are present in 40 cases of syndromic intellectual disability (Figs. 3 and 4) (*12*, *33*–*36*) and one individual with autism (*43*). As reported for H3K23 acetylation (*12*, *33*), these variants impaired BRPF1 in activating KAT6A (and perhaps also KAT6B) for H3K23 propionylation (Fig. 4). Notably, neither H3K23 acetylation nor propionylation was compromised in five patient-derived cell lines with *KAT6A* or *KAT6B* variants (fig. S8, B and D), which is expected because they contain intact MYST domains (fig. S8, A and C). A few *KAT6A* or *KAT6B* variants alter their MYST domains (*31*, *32*) and may thus affect acylation. The drugs valproate and vorinostat rescued acylation defects in cultured cells with mouse *Brpf1* (or human *BRPF1*) mutations (Fig. 6, B and C). Moreover, butyrate and propionate corrected acylation deficiency (Fig. 6, C and E). They are major end products from fermentation of dietary fiber by gut microbiota (*46*), while propionate is a nutrient supplement (marketed as Propicum).

One interesting issue is in regard to structural and functional differences between KAT6A and KAT6B (Fig. 1A). As two paralogs, they are highly homologous to each other at the sequence level (*23*) and also display similar properties in vitro, in terms of complex formation with BRPF1 and histone H3 acylation. The MYST domain of KAT6A or KAT6B had H3K23 propionyltransferase activity in vitro (Fig. 1, C and E). However, they display functional differences in vivo, in part due to their distinct expression patterns. In addition, their regulatory mechanisms may be different in vivo. Their knockout mice display distinct phenotypes (*23*), and patients with *KAT6A* or *KAT6B* variants exhibit different clinical features (*24*–*32*).

In summary, this study identifies BRPF1-KAT6 complexes as H3K23 propionyltransferases and links histone propionylation deficiency to developmental disorders and cancer. We propose that compared to acetylation, propionylation serves a complementary regulatory mechanism (Fig. 6, F and G). This study thus not only suggests targeted therapeutic strategies for medical conditions with germline (or somatic) *BRPF1*, *KAT6A*, or *KAT6B* variants but also sheds light on the metabolic disorder propionic acidemia and propionate-based nutrient supplements.

MATERIALS AND METHODS

Human individuals

Families were consented for clinical studies approved by the CHU Sainte-Justine Institutional Review Board (IRB) (Montreal, Quebec, Canada). At the Autism and Developmental Medicine Institute at Geisinger, patients are offered participation in an IRB-approved protocol that allows the use and publication of clinically obtained data (including genetic test results) to be used for research purposes. For publication of the photos in Fig. 3 and fig. S4C, informed written consent was obtained specifically.

Exome and Sanger sequencing

Clinical exome sequencing was carried out as described (*12*, *33*). Exome sequencing was carried out at a clinical genetic testing laboratory for individual P7, but parental samples were unavailable for testing.

Mice and animal study approval

Mice strains were maintained in the Comparative Medicine and Animal Resources Centre of McGill University, Montreal, Quebec, Canada. All procedures related to mouse work were performed according to an animal use protocol approved by the McGill University Animal Care Committee.

Brpf1$^{f/f}$ mice were maintained in C57BL/6J genetic background, in which the conditional *Brpf1*^{f} allele contains two LoxP sites flanking exons 4 to 6 (*39*, *55*, *56*). Breeding with *Brpf1*$^{f/f}$ mice and *UBC-Cre/ERT2* strain (The Jackson Laboratory, 007001) generated *Brpf1*$^{f/+}$*;ER-Cre* mice, which were further intercrossed to yield *Brpf1*$^{f/f}$*;ER-Cre* embryos for MEF isolation (*39*). For epiblast-specific knockouts, *Brpf1*$^{f/f}$ mice were crossed with the *Meox2-Cre* strain (The Jackson Laboratory, 003755). *Brpf1* knockout embryos (E10.5) were prepared from intercross of *Brpf1*$^{f/+}$*;Meox2-Cre* mice, as previously described (*12*). The *Kat6a*$^{f/f}$ mice line was generated in a mixed C57BL/6J-CD1 genetic background (*12*). The *Kat6a*^{f} allele contains two LoxP sites flanking the second coding exon. Crossing this mice line with the *EIIa-Cre* stain (The Jackson Laboratory, 003724) yielded *Kat6a*$^{f/+}$*;EIIa-Cre* mice, which were further intercrossed to generate *Kat6a* knockout embryos and MEFs (*57*). Knockout efficiency was verified by genomic polymerase chain reaction (PCR) and/or reverse transcription quantitative real-time PCR (*57*).

Cell lines and MEFs

HEK293 cells were maintained in Dulbecco's modified Eagle's medium (Gibco, 11995-073) supplemented with 10% heat-inactivated fetal bovine serum (Gibco, A3160702), penicillin (100 U/ml), and streptomycin (100 μg/ml). Both fibroblasts and LCLs including controls and those from patients with the Pro370Ser and Arg455* variants were prepared as described (*12*). Breast cancer MCF7 cells were cultured in the above medium. MEFs were prepared and cultured as previously described (*12*). MEFs from tamoxifen-inducible *Brpf1*^{ff}*;ER-Cre* embryos were used to obtain *Brpf1*-null MEFs after treatment with 0.25 μM 4-hydroxytamoxifen (Sigma-Aldrich, T176) for 3 days in vitro (*39*).

Downloaded from http://advances.sciencemag.org/ on February 12, 2020

Kat6a-null MEFs were prepared from *Kat6a*$^{f/f}$;*EIIa-Cre* embryos as described (*57*).

Fluorescence microscopy

For analysis of subcellular localization, expression plasmids for EGFP (enhanced green fluorescent protein)–BRPF1 and its mutants were transiently transfected into HEK293 cells with or without expression vectors for KAT6A, ING5, and MEAF6 as specified in Fig. 5D. About 16 hours after transfection, live green fluorescence signals were examined under a fluorescence microscope, and images were captured for further processing as described (*18*).

Mutagenesis and acetyltransferase complex reconstitution

All expression constructs were engineered on derivatives of the mammalian expression vector pcDNA3.1 (Invitrogen). Site-directed mutagenesis to generate expression vectors for HA-tagged BRPF1 variants corresponding to the variants identified in individuals with syndromic intellectual disability was carried out via PCR with *Pfu* Ultra High-fidelity DNA Polymerase AD (Agilent, 600385), followed by Dpn I digestion. After transformation into DH5α, plasmids were isolated from the resulting colonies for restriction digestion and further verification of the variants by Sanger DNA sequencing.

For BRPF1-KAT6 complex reconstitution in cells, an expression plasmid for FLAG-tagged KAT6A, its fragment or a KAT6B fragment was transfected into HEK293 cells along with the expression vectors for HA-tagged BRPF1, ING5, and MEAF6 as described (*18*, *21*). About 48 hours after transfection, cells were washed twice with phosphate-buffered saline (PBS), and soluble protein extracts were prepared in buffer K for affinity purification on anti-FLAG M2 agarose (Sigma-Aldrich, A2220), as previously described (*18*, *21*). After extensive washing three times with buffer K containing 0.6 M KCl and once with buffer K, the FLAG peptide (Sigma-Aldrich, F3290) was added to buffer K to elute bound proteins for immunoblotting analysis with anti-FLAG and anti-HA antibodies or for acetyltransferase activity determination. Acetylation of HeLa oligonucleosomes was performed as described (*18*, *21*). Because of no basal acylation signals detected, recombinant mononucleosomes were used for most of the assays presented here (except for Figs. 1B and 4B).

Histone acylation assays

The assays were performed as previously reported (*18*, *21*). Briefly, reconstituted KAT6 complexes were incubated with 0.2 to 1 μg of nucleosomes and 0.1 mM acetyl-CoA (Sigma-Aldrich, A2056), propionyl-CoA (Sigma-Aldrich, P5397), crotonyl-CoA (Sigma-Aldrich, 28007), or butyryl-CoA (Sigma-Aldrich, B1508) at 37°C for 1 hour. HeLa oligonucleosomes were purified as previously described (*21*), where recombinant mononucleosomes were purchased from EpiCypher (16-0009). Reactions were terminated by addition of a 3× reducing SDS sample buffer for separation by SDS–polyacrylamide gel electrophoresis (PAGE) (15%) and transferred to 0.22-μm nitrocellulose membrane (Pall Laboratory, 66485) and subsequent immunoblotting analysis to detect histone H3 or its acylation with site-specific antibodies as described below. The KAT6 complexes in the acylation reactions were verified by immunoblotting with anti-FLAG (Sigma-Aldrich, F3165) and anti-HA (BioLegend, 901515) antibodies.

Immunoblotting analysis

For assessment of endogenous histone acylation, cells and embryos were lysed in the radioimmunoprecipitation assay (RIPA) buffer [150 mM NaCl, 1.0% NP-40, 0.5% sodium deoxycholate, 0.1% SDS, 50 mM tris-HCl (pH 8.0), and protease inhibitor mixture] for immunoblotting. Histone acylation was analyzed by immunoblotting with anti-H3 (Abcam, ab1791; 1:100,000), anti-H3K9ac (Abcam, ab10812; 1:1000), anti-H3K18ac (EMD Millipore, 07-354; 1:1000), anti-H3K23ac (EMD Millipore, 07-355; 1:10,000), anti-H3K23pr (PTM Biolabs, PTM-205; 1:1000), anti-H3K23cr (PTM Biolabs, PTM-519; 1:1000), anti-H3K23bu (PTM Biolabs, PTM-307; 1:1000), anti-H3K23me3 (Active Motif, 61499; 1:1000), anti-H3K14ac (EMD Millipore, 07-353; 1:1000), anti-H3K14pr (PTM Biolabs, PTM-211; 1:1000), anti-H3K14cr (PTM Biolabs, PTM-535; 1:1000), anti-H3K14hib (PTM Biolabs, PTM-881; 1:1000), anti-propionyllysine (PTM Biolabs, PTM-201; 1:1000), anti-crotonyllysine (PTM Biolabs, PTM-502; 1:1000), and anti-succinyllysine (PTM Biolabs, PTM-402; 1:1000) antibodies in 5% nonfat milk or bovine serum albumin in the TBST (Tris-buffered saline with Tween 20) buffer for overnight at 4°C. Goat anti-Rabbit IgG (H+L)-HRP (Thermo Fisher Scientific, 65-6120) and Goat anti-Mouse IgG (H+L)-HRP (Thermo Fisher Scientific, 62-6520) were used as the secondary antibodies at a dilution of 1:5000 for blotting for 1 hour at room temperature. After extensive washing four times with the TBST buffer (7 min each), blots were developed with the Pierce ECL Western Blotting Substrate (Thermo Fisher Scientific, 32109).

Coimmunoprecipitation

Coimmunoprecipitation was carried out as described (*21*). Briefly, 25 μg of extracts from wild-type or *Brpf1*$^{-/-}$ MEFs (E13.5) was preincubated with 5 μg of antibody in the NP-40 buffer [50 mM tris-HCl (pH 8.0), 50 mM NaCl, 1% NP-40, 50 mM NaF, and protease inhibitor cocktail] with overnight rotation at 4°C. Immunoprecipitation was then performed by incubating each mixture with 25 μl of Dynabeads Protein G (Invitrogen, 10003D) with rotation for 45 min at 4°C. After washing four times with 0.5 ml of PBS containing 0.02% Tween 20 and protease inhibitor cocktail, the Dynabeads were resuspended in the reducing SDS sample buffer and boiled for 5 min. The supernatant was used for SDS-PAGE and immunoblotting analysis with the indicated antibodies.

Pharmacological treatment

Cells were seeded so that they would reach at ~90% confluency on the following day. After one wash with PBS, cells were treated with the medium supplemented with the vehicle solvent, sodium propionate (Sigma-Aldrich, P5436), sodium valproate (Sigma-Aldrich, P4543), SAHA (Sigma-Aldrich, SML0061), β-hydroxybutyrate (Sigma-Aldrich, H6501), TSA (Sigma-Aldrich, T8552), sodium butyrate (Sigma-Aldrich, B5887), or HDAC3 inhibitor RGFP966 (Selleckchem, S7229) for 24 hours. Cells were washed with PBS and lysed in the RIPA buffer (Thermo Fisher Scientific, 89900) to prepare soluble protein extracts or in the Triton extraction buffer (PBS containing 0.5% Triton X-100, 2 mM phenylmethylsulfonyl fluoride, 0.02% NaN_3, and protease inhibitors) to prepare protein extracts. Extracts were prepared in buffer K and further analyzed by immunoblotting with various antibodies as described above.

ATAC-See and immunofluorescence microscopy

The ATAC-See procedure was modified from a published report on cells (*58*) to obtain more reliable results for cultured cells and extend the application to paraffinized tissue sections. The isopropyl-β-D-thiogalactopyranoside (IPTG)–inducible expression vector pTXB1-Tn5 was obtained from Addgene (60240). Hyperactive Tn5 was

Downloaded from http://advances.sciencemag.org/ on February 12, 2020

bacterially expressed and affinity-purified according to a published procedure (*59*). On the basis of SDS-PAGE and Colloidal Coomassie blue staining, purified Tn5 protein was adjusted to ~1 mg/ml. The Tn5 adaptor ATTO633-Tn5ME/Tn5MErev was assembled from the ATTO-633 N-labeled oligo (/5ATTO633N/TCGTCGGCAGCGTCAGATGTGTATAAGAGACAG) and the Tn5MErev oligo (/5Phos/CTGTCTCTTATACACATCT) (*58*). The Tn5 transposome was assembled from 2 μl of Tn5 protein, 0.2 μl of the Tn5 adaptor ATTO633-Tn5ME/Tn5MErev (12.5 μM/each oligo), 2 μl of 50% glycerol, and 0.8 μl of H_2O. After incubation at room temperature for 1 hour, the assembled Tn5 transposome was stored shortly at 4°C for transposition reactions.

For ATAC-See, MEFs were grown on round coverslips in wells of a 12-well plate. At 80 to 90% confluency, cells were fixed with 1% formaldehyde (Sigma-Aldrich, F8775) for 10 min at room temperature. After fixation, the cells were permeabilized with the modified lysis buffer [10 mM tris-Cl (pH 7.4), 10 mM NaCl, 3 mM $MgCl_2$, and 0.2% Triton X-100] for 10 min at room temperature. Paraffinized control and *Kat6a*$^{-/-}$;*EIIa-Cre* embryo sections were deparaffinized for antigen retrieval as previously described (*39*, *55*, *56*) and permeabilized with the modified lysis buffer for 10 min at room temperature. After permeabilization, coverslips or embryo sections were rinsed twice in PBS.

For transposition reactions, the assembled Tn5 transposome was mixed with 25 μl of 2× tagmentation buffer [33 mM tris-acetate (pH 7.8), 66 mM potassium acetate, 11 mM magnesium acetate, and 16% *N*,*N*-dimethylformamide] and 20 μl of H_2O. The mixture was added onto coverslips or embryo sections for incubation at 37°C for 60 min. After transposition reactions, coverslips were washed thrice with the washing buffer (0.01% SDS and 50 mM EDTA in PBS) at 55°C. For paraffinized tissue sections, a modified washing buffer (0.5% SDS, 100 mM EDTA, and 0.25 M NaCl in PBS) was used to reduce autofluorescence background. After ATAC-See, immunofluorescence microscopy using antibodies specific to histone or its modified forms was carried out as described (*39*, *55*, *56*). Alexa Fluor 488–conjugated anti-rabbit immunoglobulin G (IgG) (Invitrogen, A-11034) and Alexa Fluor 488–conjugated anti-mouse IgG (Invitrogen, A-11001) were used as the secondary antibodies.

Sequence alignment

The sequence similarity with Sfp1 was initially noticed during BLAST search using the C2H2 zinc finger region of BRPF1 as bait, with a *P* value of 3×10^{-4}. GenBank accession numbers used for the alignment in Fig. 5B are P55201 (BRPF1), NP_001286155 (Br140), NP_013507 (Sfp1), NP_651853 (CG12054), XP_006715719 (JAZF1), and XP_011519688 (ZF609). Asterisks denote Cys and His residues that may be involved in chelating zinc for zinc finger formation; His47 may replace His44 for zinc chelating. The known or potential DNA-recognizing residues at three key positions (*60*) are highlighted in bold (Fig. 5B). The sequence alignment was generated with the ClustIW module of a MacVector software package (version 11.10.2).

SUPPLEMENTAL MATERIALS

Supplementary material for this article is available at http://advances.sciencemag.org/cgi/content/full/6/4/eaax0021/DC1

Fig. S1. Analysis of histone H3K23 acylation–specific antibodies.
Fig. S2. Impact of BRPF1 and its mutants on expression of ING5 and MEAF6.
Fig. S3. Histone H3 acylation in cultured cells and E10.5 mouse embryos.
Fig. S4. Fluorescence microscopic images of H3K23 acylation in mouse embryos and photographs of two individuals with heterozygous *BRPF1* variants.
Fig. S5. Comparison of human BRPF1 with its orthologs from different organisms.
Fig. S6. Sequence similarity among the PWWP domains of human BRPF1 and its orthologs from different organisms.
Fig. S7. Three-dimensional location of representative variants and analysis of the Pro76Leu variant.
Fig. S8. H3K23 acylation in LCLs derived from patients with *KAT6A* or *KAT6B* variants.
Fig. S9. Distribution of cancer-derived somatic *BRPF1* mutations.
Table S1. *BRPF1* variants and clinical information in 12 previously unreported cases.

View/request a protocol for this paper from *Bio-protocol*.

REFERENCES AND NOTES

1. C. D. Allis, T. Jenuwein, The molecular hallmarks of epigenetic control. *Nat. Rev. Genet.* **17**, 487–500 (2016).
2. A. Dutta, S. M. Abmayr, J. L. Workman, Diverse activities of histone acylations connect metabolism to chromatin function. *Mol. Cell* **63**, 547–552 (2016).
3. B. R. Sabari, D. Zhang, C. D. Allis, Y. Zhao, Metabolic regulation of gene expression through histone acylations. *Nat. Rev. Mol. Cell Biol.* **18**, 90–101 (2017).
4. X. Xiong, T. Panchenko, S. Yang, S. Zhao, P. Yan, W. Zhang, W. Xie, Y. Li, Y. Zhao, C. D. Allis, H. Li, Selective recognition of histone crotonylation by double PHD fingers of MOZ and DPF2. *Nat. Chem. Biol.* **12**, 1111–1118 (2016).
5. F. H. Andrews, S. A. Shinsky, E. K. Shanle, J. B. Bridgers, A. Gest, I. K. Tsun, K. Krajewski, X. Shi, B. D. Strahl, T. G. Kutateladze, The Taf14 YEATS domain is a reader of histone crotonylation. *Nat. Chem. Biol.* **12**, 396–398 (2016).
6. Y. Li, B. R. Sabari, T. Panchenko, H. Wen, D. Zhao, H. Guan, L. Wan, H. Huang, Z. Tang, Y. Zhao, R. G. Roeder, X. Shi, C. D. Allis, H. Li, Molecular coupling of histone crotonylation and active transcription by AF9 YEATS domain. *Mol. Cell* **62**, 181–193 (2016).
7. B. J. Klein, J. Simithy, X. Wang, J. Ahn, F. H. Andrews, Y. Zhang, J. Côté, X. Shi, B. A. Garcia, T. G. Kutateladze, Recognition of histone H3K14 acylation by MORF. *Structure* **25**, 650–654.e2 (2017).
8. X.-J. Yang, The diverse superfamily of lysine acetyltransferases and their roles in leukemia and other diseases. *Nucleic Acids Res.* **32**, 959–976 (2004).
9. C. D. Allis, S. L. Berger, J. Cote, S. Dent, T. Jenuwien, T. Kouzarides, L. Pillus, D. Reinberg, Y. Shi, R. Shiekhattar, A. Shilatifard, J. Workman, Y. Zhang, New nomenclature for chromatin-modifying enzymes. *Cell* **131**, 633–636 (2007).
10. F. Huang, A. Paulson, A. Dutta, S. Venkatesh, M. Smolle, S. M. Abmayr, J. L. Workman, Histone acetyltransferase Enok regulates oocyte polarization by promoting expression of the actin nucleation factor spire. *Genes Dev.* **28**, 2750–2763 (2014).
11. L. You, L. Li, J. Zou, K. Yan, J. Belle, A. Nijnik, E. Wang, X.-J. Yang, BRPF1 is essential for development of fetal hematopoietic stem cells. *J. Clin. Invest.* **126**, 3247–3262 (2016).
12. K. Yan, J. Rousseau, R. O. Littlejohn, C. Kiss, A. Lehman, J. R. Rosenfeld, C. T. R. Stumpel, A. P. Stegmann, L. Robak, F. Scaglia, T. T. Nguyen, H. Fu, N. F. Ajeawung, M. V. Camurri, L. Li, A. Gardham, B. Panis, M. Almannai, M. J. Guillen Sacoto, B. Baskin, C. Ruivenkamp, F. Xia, W. Bi; DDD Study; CAUSES Study, M. T. Cho, T. P. Potjer, G. W. E. Santen, M. J. Parker, N. Canham, M. McKinnon, L. Potocki, J. MacKenzie, E. R. Roeder, P. M. Campeau, X.-J. Yang, Mutations in the chromatin regulator gene BRPF1 causes syndromic intellectual disability and deficient histone acetylation. *Am. J. Hum. Genet.* **100**, 91–104 (2017).
13. T. Thomas, M. P. Dixon, A. J. Kueh, A. K. Voss, Mof (MYST1 or KAT8) is essential for progression of embryonic development past the blastocyst stage and required for normal chromatin architecture. *Mol. Cell. Biol.* **28**, 5093–5105 (2008).
14. G. G. Sharma, S. So, A. Gupta, R. Kumar, C. Cayrou, N. Avvakumov, U. Bhadra, R. K. Pandita, M. H. Porteus, D. J. Chen, J. Cote, T. K. Pandita, MOF and histone H4 acetylation at lysine 16 are critical for DNA damage response and double-strand break repair. *Mol. Cell. Biol.* **30**, 3582–3595 (2010).
15. X. Li, C. A. Corsa, P. W. Pan, L. Wu, D. Ferguson, X. Yu, J. Min, Y. Dou, MOF and H4 K16 acetylation play important roles in DNA damage repair by modulating recruitment of DNA damage repair protein Mdc1. *Mol. Cell. Biol.* **30**, 5335–5347 (2010).
16. A. J. Kueh, M. P. Dixon, A. K. Voss, T. Thomas, HBO1 is required for H3K14 acetylation and normal transcriptional activity during embryonic development. *Mol. Cell. Biol.* **31**, 845–860 (2011).
17. Y. Mishima, S. Miyagi, A. Saraya, M. Negishi, M. Endoh, T. A. Endo, T. Toyoda, J. Shinga, T. Katsumoto, T. Chiba, N. Yamaguchi, I. Kitabayashi, H. Koseki, A. Iwama, The Hbo1-Brd1/Brpf2 complex is responsible for global acetylation of H3K14 and required for fetal liver erythropoiesis. *Blood* **118**, 2443–2453 (2011).
18. K. Yan, L. You, C. Degerny, M. Ghorbani, X. Liu, L. Chen, L. Li, D. Miao, X.-J. Yang, The chromatin regulator BRPF3 preferentially activates the HBO1 acetyltransferase but is dispensable for mouse development and survival. *J. Biol. Chem.* **291**, 2647–2663 (2016).
19. Y. Feng, A. Vlassis, C. Roques, M.-E. Lalonde, C. González-Aguilera, J.-P. Lambert, S.-B. Lee, X. Zhao, C. Alabert, J. V. Johansen, E. Paquet, X.-J. Yang, A.-C. Gingras, J. Côté, A. Groth, BRPF3-HBO1 regulates replication origin activation and histone H3K14 acetylation. *EMBO J.* **35**, 176–192 (2016).

Downloaded from http://advances.sciencemag.org/ on February 12, 2020

20. Y. Doyon, C. Cayrou, M. Ullah, A.-J. Landry, V. Côté, W. Selleck, W. S. Lane, S. Tan, X.-J. Yang, J. Côté, ING tumor suppressor proteins are critical regulators of chromatin acetylation required for genome expression and perpetuation. *Mol. Cell* **21**, 51–64 (2006).
21. M. Ullah, N. Pelletier, L. Xiao, S. P. Zhao, K. Wang, C. Degerny, S. Tahmasebi, C. Cayrou, Y. Doyon, S.-L. Goh, N. Champagne, J. Côté, X.-J. Yang, Molecular architecture of quartet MOZ/MORF histone acetyltransferase complexes. *Mol. Cell. Biol.* **28**, 6828–6843 (2008).
22. M.-E. Lalonde, N. Avakumov, K. C. Glass, F.-H. Joncas, N. Saksouk, M. Holliday, E. Paquet, K. Yan, Q. Tong, B. J. Klein, S. Tan, X.-J. Yang, T. G. Kutateladze, J. Côté, Exchange of associated factors directs a switch in HBO1 acetyltransferase histone tail specificity. *Genes Dev.* **27**, 2009–2024 (2013).
23. X. J. Yang, MOZ and MORF acetyltransferases: Molecular interaction, animal development and human disease. *Biochim. Biophys. Acta* **1853**, 1818–1826 (2015).
24. M. Kraft, I. C. Cirstea, A. K. Voss, T. Thomas, I. Goehring, B. N. Sheikh, L. Gordon, H. Scott, G. K. Smyth, M. R. Ahmadian, U. Trautmann, M. Zenker, M. Tartaglia, A. Ekici, A. Reis, H.-G. Dörr, A. Rauch, C. T. Thiel, Disruption of the histone acetyltransferase MYST4 leads to a Noonan syndrome-like phenotype and hyperactivated MAPK signaling in humans and mice. *J. Clin. Invest.* **121**, 3479–3491 (2011).
25. J. Clayton-Smith, J. O'Sullivan, S. Daly, S. Bhaskar, R. Day, B. Anderson, A. K. Voss, T. Thomas, L. G. Biesecker, P. Smith, A. Fryer, K. E. Chandler, B. Kerr, M. Tassabehji, S.-A. Lynch, M. Krajewska-Walasek, S. McKee, J. Smith, E. Sweeney, S. Mansour, S. Mohammed, D. Donnai, G. Black, Whole-exome-sequencing identifies mutations in histone acetyltransferase gene KAT6B in individuals with the Say-Barber-Biesecker variant of Ohdo syndrome. *Am. J. Hum. Genet.* **89**, 675–681 (2011).
26. M. A. Simpson, C. Deshpande, D. Dafou, L. E. Vissers, W. J. Woollard, S. E. Holder, G. Gillessen-Kaesbach, R. Derks, S. M. White, R. Cohen-Snuijf, S. G. Kant, L. H. Hoefsloot, W. Reardon, H. G. Brunner, E. M. Bongers, R. C. Trembath, De novo mutations of the gene encoding the histone acetyltransferase KAT6B cause genitopatellar syndrome. *Am. J. Hum. Genet.* **90**, 290–294 (2012).
27. P. M. Campeau, J. C. Kim, J. T. Lu, J. A. Schwartzentruber, O. A. Abdul-Rahman, S. Schlaubitz, D. M. Murdock, M.-M. Jiang, E. J. Lammer, G. M. Enns, W. J. Rhead, J. Rowland, S. P. Robertson, V. Cormier-Daire, M. N. Bainbridge, X.-J. Yang, M.-C. Gingras, R. A. Gibbs, D. S. Rosenblatt, J. Majewski, B. H. Lee, Mutations in KAT6B, encoding a histone acetyltransferase, cause genitopatellar syndrome. *Am. J. Hum. Genet.* **90**, 282–289 (2012).
28. H.-C. Yu, E. A. Geiger, L. Medne, E. H. Zackai, T. H. Shaikh, An individual with blepharophimosis–ptosis–epicanthus inversus syndrome (BPES) and additional features expands the phenotype associated with mutations in KAT6B. *Am. J. Med. Genet. A* **164**, 950–957 (2014).
29. V. A. Arboleda, H. Lee, N. Dorrani, N. Zadeh, M. Willis, C. F. Macmurdo, M. A. Manning, A. Kwan, L. Hudgins, F. Barthelemy, M. C. Miceli, F. Quintero-Rivera, S. Kantarci, S. P. Strom, J. L. Deignan; UCLA Clinical Genomics Center, W. W. Grody, E. Vilain, S. F. Nelson, De novo nonsense mutations in KAT6A, a lysine acetyl-transferase gene, cause a syndrome including microcephaly and global developmental delay. *Am. J. Hum. Genet.* **96**, 498–506 (2015).
30. E. Tham, A. Lindstrand, A. Santani, H. Malmgren, A. Nesbitt, H. A. Dubbs, E. H. Zackai, M. J. Parker, F. Millan, K. Rosenbaum, G. N. Wilson, A. Nordgren, Dominant mutations in KAT6A cause intellectual disability with recognizable syndromic features. *Am. J. Hum. Genet.* **96**, 507–513 (2015).
31. J. Kennedy, D. Goudie, E. Blair, K. Chandler, S. Joss, V. McKay, A. Green, R. Armstrong, M. Lees, B. Kamien, B. Hopper, T. Y. Tan, P. Yap, Z. Stark, N. Okamoto, N. Miyake, N. Matsumoto, E. Macnamara, J. L. Murphy, E. McCormick, H. Hakonarson, M. J. Falk, D. Li, P. Blackburn, E. Klee, D. Babovic-Vuksanovic, S. Schelley, L. Hudgins, S. Kant, B. Isidor, B. Cogne, K. Bradbury, M. Williams, C. Patel, H. Heussler, C. Duff-Farrier, P. Lakeman, I. Scurr, U. Kini, M. Elting, M. Reijnders, J. Schuurs-Hoeijmakers, M. Wafik, A. Blomhoff, C. A. L. Ruivenkamp, E. Nibbeling, A. J. M. Dingemans, E. D. Douine, S. F. Nelson; DDD Study, V. A. Arboleda, R. Newbury-Ecob, KAT6A syndrome: Genotype–phenotype correlation in 76 patients with pathogenic KAT6A variants. *Genet. Med.* **21**, 850–860 (2019).
32. A. Brea-Fernández, D. Dacruz, J. Eirís, F. Barros, Á. Carracedo, Novel truncating variants expand the phenotypic spectrum of KAT6B-related disorders. *Am. J. Med. Genet. A* **179**, 290–294 (2019).
33. F. Mattioli, E. Schaefer, A. Magee, P. Mark, G. M. Mancini, K. Dieterich, G. Von Allmen, M. Alders, C. Coutton, M. van Slegtenhorst, G. Vieville, M. Engelen, J. M. Cobben, J. Juusola, A. Pujol, J.-L. Mandel, A. Piton, Mutations in histone acetylase modifier BRPF1 cause an autosomal-dominant form of intellectual disability with associated ptosis. *Am. J. Hum. Genet.* **100**, 105–116 (2017).
34. S. Baker, J. Murrell, A. Nesbitt, K. Pechter, J. Balciuniene, X. Zhao, Z. Yu, E. H. Denenberg, E. T. DeChene, A. B. Wilkens, E. J. Bhoj, Q. Guan, M. C. Dulik, L. K. Conlin, A. N. Abou Tayoun, M. Luo, C. Wu, K. Cao, M. Sarmady, E. C. Bedoukian, J. Tarpinian, L. Medne, C. M. Skraban, M. A. Deardorff, I. D. Krantz, B. L. Krock, A. B. Santani, Automated clinical exome reanalysis reveals novel diagnoses. *J. Mol. Diagn.* **21**, 38–48 (2019).
35. N. Pode-Shakked, O. Barel, B. Pode-Shakked, A. Eliyahu, A. Singer, O. Nayshool, N. Kol, A. Raas-Rothschild, E. Pras, M. Shohat, BRPF1-associated intellectual disability, ptosis, and facial dysmorphism in a multiplex family. *Mol. Genet. Genomic Med.* **7**, e665 (2019).
36. S. Demeulenaere, D. Beysen, I. De Veuster, E. Reyniers, F. Kooy, M. Meuwissen, Novel BRPF1 mutation in a boy with intellectual disability, coloboma, facial nerve palsy and hypoplasia of the corpus callosum. *Eur. J. Med. Genet.* **62**, 103691 (2019).
37. H. Yuan, D. Rossetto, H. Mellert, W. Dang, M. Srinivasan, J. Johnson, S. Hodawadekar, E. C. Ding, K. Speicher, N. Abshiru, R. Perry, J. Wu, C. Yang, Y. G. Zheng, D. W. Speicher, P. Thibault, A. Verreault, F. B. Johnson, S. L. Berger, R. Sternglanz, S. B. McMahon, J. Côté, R. Marmorstein, MYST protein acetyltransferase activity requires active site lysine autoacetylation. *EMBO J.* **31**, 58–70 (2012).
38. J. Borrow, V. P. Stanton Jr., J. M. Andresen, R. Becher, F. G. Behm, R. S. Chaganti, C. I. Civin, C. Disteche, I. Dubé, A. M. Frischauf, D. Horsman, F. Mitelman, S. Volinia, A. E. Watmore, D. E. Housman, The translocation t(8;16)(p11;p13) of acute myeloid leukaemia fuses a putative acetyltransferase to the CREB–binding protein. *Nat. Genet.* **14**, 33–41 (1996).
39. L. You, K. Yan, J. Zou, H. Zhao, N. R. Bertos, M. Park, E. Wang, X.-J. Yang, The chromatin regulator Brpf1 regulates embryo development and cell proliferation. *J. Biol. Chem.* **290**, 11349–11364 (2015).
40. X. Chen, Y. Shen, W. Draper, J. D. Buenrostro, U. Litzenburger, S. W. Cho, A. T. Satpathy, A. C. Carter, R. P. Ghosh, A. East-Seletsky, J. A. Doudna, W. J. Greenleaf, J. T. Liphardt, H. Y. Chang, ATAC-see reveals the accessible genome by transposase-mediated imaging and sequencing. *Nat. Methods* **13**, 1013–1020 (2016).
41. A. Vezzoli, N. Bonadies, M. D. Allen, S. M. Freund, C. M. Santiveri, B. T. Kvinlaug, B. J. Huntly, B. Göttgens, M. Bycroft, Molecular basis of histone H3K36me3 recognition by the PWWP domain of Brpf1. *Nat. Struct. Mol. Biol.* **17**, 617–619 (2010).
42. H. Wu, H. Zeng, R. Lam, W. Tempel, M. F. Amaya, C. Xu, L. Dombrovski, W. Qiu, Y. Wang, J. Min, Structural and histone binding ability characterizations of human PWWP domains. *PLOS ONE* **6**, e18919 (2011).
43. I. Iossifov, B. J. O'Roak, S. J. Sanders, M. Ronemus, N. Krumm, D. Levy, H. A. Stessman, K. T. Witherspoon, L. Vives, K. E. Patterson, J. D. Smith, B. Paeper, D. A. Nickerson, J. Dea, S. Dong, L. E. Gonzalez, J. D. Mandell, S. M. Mane, M. T. Murtha, C. A. Sullivan, M. F. Walker, Z. Waqar, L. Wei, A. J. Willsey, B. Yamrom, Y.-h. Lee, E. Grabowska, E. Dalkic, Z. Wang, S. Marks, P. Andrews, A. Leotta, J. Kendall, I. Hakker, J. Rosenbaum, B. Ma, L. Rodgers, J. Troge, G. Narzisi, S. Yoon, M. C. Schatz, K. Ye, W. R. McCombie, J. Shendure, E. E. Eichler, M. W. State, M. Wigler, The contribution of de novo coding mutations to autism spectrum disorder. *Nature* **515**, 216–221 (2014).
44. M. Kool, D. T. Jones, N. Jäger, P. A. Northcott, T. J. Pugh, V. Hovestadt, R. M. Piro, L. A. Esparza, S. L. Markant, M. Remke, T. Milde, F. Bourdeaut, M. Ryzhova, D. Sturm, E. Pfaff, S. Stark, S. Hutter, H. Şeker-Cin, P. Johann, S. Bender, C. Schmidt, T. Rausch, D. Shih, J. Reimand, L. Sieber, A. Wittmann, L. Linke, H. Witt, U. D. Weber, M. Zapatka, R. König, R. Beroukhim, G. Bergthold, P. van Sluis, R. Volckmann, J. Koster, R. Versteeg, S. Schmidt, S. Wolf, C. Lawerenz, C. C. Bartholomae, C. von Kalle, A. Unterberg, C. Herold-Mende, S. Hofer, A. E. Kulozik, A. von Deimling, W. Scheurlen, J. Felsberg, G. Reifenberger, M. Hasselblatt, J. R. Crawford, G. A. Grant, N. Jabado, A. Perry, C. Cowdrey, S. Croul, G. Zadeh, J. O. Korbel, F. Doz, O. Delattre, G. D. Bader, M. G. McCabe, V. P. Collins, M. W. Kieran, Y.-J. Cho, S. L. Pomeroy, O. Witt, B. Brors, M. D. Taylor, U. Schüller, A. Korshunov, R. Eils, R. J. Wechsler-Reya, P. Lichter, S. M. Pfister; ICGC PedBrain Tumor Project, Genome sequencing of SHH medulloblastoma predicts genotype-related response to smoothened inhibition. *Cancer Cell* **25**, 393–405 (2014).
45. R. Huether, L. Dong, X. Chen, G. Wu, M. Parker, L. Wei, J. Ma, M. N. Edmonson, E. K. Hedlund, M. C. Rusch, S. A. Shurtleff, H. L. Mulder, K. Boggs, B. Vadordaria, J. Cheng, D. Yergeau, G. Song, J. Becksfort, G. Lemmon, C. Weber, Z. Cai, J. Dang, M. Walsh, A. L. Gedman, Z. Faber, J. Easton, T. Gruber, R. W. Kriwacki, J. F. Partridge, L. Ding, R. K. Wilson, E. R. Mardis, C. G. Mullighan, R. J. Gilbertson, S. J. Baker, G. Zambetti, D. W. Ellison, J. Zhang, J. R. Downing, The landscape of somatic mutations in epigenetic regulators across 1,000 paediatric cancer genomes. *Nat. Commun.* **5**, 3630 (2014).
46. A. Koh, F. De Vadder, P. Kovatcheva-Datchary, F. Bäckhed, From dietary fiber to host physiology: Short-chain fatty acids as key bacterial metabolites. *Cell* **165**, 1332–1345 (2016).
47. X.-J. Yang, E. Seto, The Rpd3/Hda1 family of lysine deacetylases: From bacteria and yeast to mice and men. *Nat. Rev. Mol. Cell Biol.* **9**, 206–218 (2008).
48. D. P. Johnson, G. S. Spitz, S. Tharkar, S. N. Quayle, J. R. Shearstone, S. Jones, M. E. McDowell, H. Wellman, J. K. Tyler, B. R. Cairns, M. B. Chandrasekharan, S. Bhaskara, HDAC1,2 inhibition impairs EZH2- and BBAP-mediated DNA repair to overcome chemoresistance in EZH2 gain-of-function mutant diffuse large B-cell lymphoma. *Oncotarget* **6**, 4863–4887 (2015).
49. A. F. Kebede, A. Nieborak, L. Z. Shahidian, S. Le Gras, F. Richter, D. A. Gómez, M. P. Baltissen, G. Meszaros, H. F. Magliarelli, A. Taudt, R. Margueron, M. Colomé-Tatché, R. Ricci, S. Daujat, M. Vermeulen, G. Mittler, R. Schneider, Histone propionylation is a mark of active chromatin. *Nat. Struct. Mol. Biol.* **24**, 1048–1056 (2017).
50. B. R. Sabari, Z. Tang, H. Huang, V. Yong-Gonzalez, H. Molina, H. E. Kong, L. Dai, M. Shimada, J. R. Cross, Y. Zhao, R. G. Roeder, C. D. Allis, Intracellular crotonyl-CoA

Downloaded from http://advances.sciencemag.org/ on February 12, 2020

stimulates transcription through p300-catalyzed histone crotonylation. *Mol. Cell* **58**, 203–215 (2015).
51. S. Sadhukhan, X. Liu, D. Ryu, O. D. Nelson, J. A. Stupinski, Z. Li, W. Chen, S. Zhang, R. S. Weiss, J. W. Locasale, J. Auwerx, H. Lin, Metabolomics-assisted proteomics identifies succinylation and SIRT5 as important regulators of cardiac function. *Proc. Natl. Acad. Sci. U.S.A.* **113**, 4320–4325 (2016).
52. K. Ravn, M. Chloupkova, E. Christensen, N. J. Brandt, H. Simonsen, J. P. Kraus, I. M. Nielsen, F. Skovby, M. Schwartz, High incidence of propionic acidemia in greenland is due to a prevalent mutation, 1540insCCC, in the gene for the β-subunit of propionyl CoA carboxylase. *Am. J. Hum. Genet.* **67**, 203–206 (2000).
53. O. Pougovkina, H. te Brinke, R. J. Wanders, S. M. Houten, V. C. de Boer, Aberrant protein acylation is a common observation in inborn errors of acyl-CoA metabolism. *J. Inherit. Metab. Dis.* **37**, 709–714 (2014).
54. L. Yu, Y. Liang, X. Cao, X. Wang, H. Gao, S.-Y. Lin, R. Schiff, X.-S. Wang, K. Li, Identification of MYST3 as a novel epigenetic activator of ERα frequently amplified in breast cancer. *Oncogene* **36**, 2910–2918 (2017).
55. L. You, J. Zou, H. Zhao, N. R. Bertos, M. Park, E. Wang, X.-J. Yang, Deficiency of the chromatin regulator Brpf1 causes abnormal brain development. *J. Biol. Chem.* **290**, 7114–7129 (2015).
56. L. You, K. Yan, J. Zou, H. Zhao, N. R. Bertos, M. Park, E. Wang, X.-J. Yang, The lysine acetyltransferase activator Brpf1 governs dentate gyrus development through neural stem cells and progenitors. *PLOS Genet.* **11**, e1005034 (2015).
57. L. You, L. Chen, J. Penney, D. Miao, X.-J. Yang, Expression atlas of the multivalent epigenetic regulator Brpf1 and its requirement for survival of mouse embryos. *Epigenetics* **9**, 860–872 (2014).
58. M. R. Corces, A. E. Trevino, E. G. Hamilton, P. G. Greenside, N. A. Sinnott-Armstrong, S. Vesuna, A. T. Satpathy, A. J. Rubin, K. S. Montine, B. Wu, A. Kathiria, S. W. Cho, M. R. Mumbach, A. C. Carter, M. Kasowski, L. A. Orloff, V. I. Risca, A. Kundaje, P. A. Khavari, T. J. Montine, W. J. Greenleaf, H. Y. Chang, An improved ATAC-seq protocol reduces background and enables interrogation of frozen tissues. *Nat. Methods* **14**, 959–962 (2017).
59. S. Picelli, Å. K. Björklund, B. Reinius, S. Sagasser, G. Winberg, R. Sandberg, Tn5 transposase and tagmentation procedures for massively scaled sequencing projects. *Genome Res.* **24**, 2033–2040 (2014).
60. A. Gupta, R. G. Christensen, H. A. Bell, M. Goodwin, R. Y. Patel, M. Pandey, M. S. Enuameh, A. L. Rayla, C. Zhu, S. Thibodeau-Beganny, M. H. Brodsky, J. K. Joung, S. A. Wolfe, G. D. Stormo, An improved predictive recognition model for Cys_2-His_2 zinc finger proteins. *Nucleic Acids Res.* **42**, 4800–4812 (2014).

Acknowledgments
Funding: This project was supported, in part, by operating grants from Canadian Institutes of Health Research (CIHR; to P.M.C. and X.-J.Y.), Natural Sciences and Engineering Research Council of Canada (NSERC; to X.-J.Y.), and Cancer Research Society (to X.-J.Y.). E.D.B. and B.C. are senior clinical investigators, and H.V. is a postdoctoral fellow of the Research Foundation–Flanders.
Author contributions: K.Y. carried out all experiments, performed data analysis, and drafted the manuscript. J.R. produced patient-derived cell lines. K.M., L.A.C., K.E.A., C.F.G., A.G., K.L.E., H.V., E.D.B., L.P., D.Z., M.C.-D., G.A.B., M.D.W., R.J.H., N.E., A.F.R., B.D.S., M.T.C., K.M., R.E., M.K.H., B.A.M., H.M.P., B.C.L., A.M.L., J.S., I.T., and B.C. identified patients and obtained clinical data. P.M.C. supervised the clinical studies and helped finalize the manuscript. X.-J.Y. supervised the project and finalized the manuscript. **Competing interests:** N.E. is affiliated with KAT6A Foundation, a newly established nonprofit organization. B.D.S., M.T.C., and K.M. are employees of GeneDx Inc., a wholly owned subsidiary of OPKO Health Inc., USA. The other authors declare that they have no competing interests. **Data and materials availability:** All data needed to evaluate the conclusions in the paper are present in the paper and/or the Supplementary Materials. Additional data related to this paper may be requested from the authors.

Submitted 13 February 2019
Accepted 20 November 2019
Published 22 January 2020
10.1126/sciadv.aax0021

Citation: K. Yan, J. Rousseau, K. Machol, L. A. Cross, K. E. Agre, C. F. Gibson, A. Goverde, K. L. Engleman, H. Verdin, E. De Baere, L. Potocki, D. Zhou, M. Cadieux-Dion, G. A. Bellus, M. D. Wagner, R. J. Hale, N. Esber, A. F. Riley, B. D. Solomon, M. T. Cho, K. McWalter, R. Eyal, M. K. Hainlen, B. A. Mendelsohn, H. M. Porter, B. C. Lanpher, A. M. Lewis, J. Savatt, I. Thiffault, B. Callewaert, P. M. Campeau, X.-J. Yang, Deficient histone H3 propionylation by BRPF1-KAT6 complexes in neurodevelopmental disorders and cancer. *Sci. Adv.* **6**, eaax0021 (2020).

Downloaded from http://advances.sciencemag.org/ on February 12, 2020

Science Advances

Deficient histone H3 propionylation by BRPF1-KAT6 complexes in neurodevelopmental disorders and cancer

Kezhi Yan, Justine Rousseau, Keren Machol, Laura A. Cross, Katherine E. Agre, Cynthia Forster Gibson, Anne Goverde, Kendra L. Engleman, Hannah Verdin, Elfride De Baere, Lorraine Potocki, Dihong Zhou, Maxime Cadieux-Dion, Gary A. Bellus, Monisa D. Wagner, Rebecca J. Hale, Natacha Esber, Alan F. Riley, Benjamin D. Solomon, Megan T. Cho, Kirsty McWalter, Roy Eyal, Meagan K. Hainlen, Bryce A. Mendelsohn, Hillary M. Porter, Brendan C. Lanpher, Andrea M. Lewis, Juliann Savatt, Isabelle Thiffault, Bert Callewaert, Philippe M. Campeau and Xiang-Jiao Yang

Sci Adv **6** (4), eaax0021.
DOI: 10.1126/sciadv.aax0021

ARTICLE TOOLS http://advances.sciencemag.org/content/6/4/eaax0021

SUPPLEMENTARY MATERIALS http://advances.sciencemag.org/content/suppl/2020/01/17/6.4.eaax0021.DC1

REFERENCES This article cites 60 articles, 15 of which you can access for free
http://advances.sciencemag.org/content/6/4/eaax0021#BIBL

PERMISSIONS http://www.sciencemag.org/help/reprints-and-permissions

Use of this article is subject to the Terms of Service

Science Advances (ISSN 2375-2548) is published by the American Association for the Advancement of Science, 1200 New York Avenue NW, Washington, DC 20005. The title *Science Advances* is a registered trademark of AAAS.

Copyright © 2020 The Authors, some rights reserved; exclusive licensee American Association for the Advancement of Science. No claim to original U.S. Government Works. Distributed under a Creative Commons Attribution NonCommercial License 4.0 (CC BY-NC).

Downloaded from http://advances.sciencemag.org/ on February 12, 2020